

1 Local moisture recycling across the globe

2 Jolanda J.E. Theeuwen^{1,2}, Arie Staal¹, Obbe A. Tuinenburg¹, Bert V.M. Hamelers^{2,3}, Stefan C. Dekker¹

3 ¹Copernicus Institute of Sustainable Development, Utrecht University, Utrecht, 3584 CB, The Netherlands

4 ²Wetsus, European Centre of Excellence for Sustainable Water Technology, Leeuwarden, 8911 MA, The Netherlands

5 ³Department of Environmental Technology, Wageningen University and Research, Wageningen, 6708 PB, The Netherlands

6 *Correspondence to:* Jolanda J.E. Theeuwen (j.j.e.theeuwen@uu.nl)

7 **Abstract.** Changes in evaporation over land affect terrestrial precipitation via atmospheric moisture recycling and
8 consequently freshwater availability. Although global moisture recycling at regional and continental scales are relatively well
9 understood, the patterns [of local moisture recycling](#) and [the main variables that impact drivers of local moisture recycling it](#)
10 remain unknown. For the first time, we calculate the local moisture recycling ratio (LMR), ~~defined~~ as the fraction of evaporated
11 moisture that ~~rains out-precipitates~~ within [a distance of 0.5° \(approximately typically 50 km\)](#) from its source, ~~and~~ identify ~~its~~
12 ~~drivers~~ [variables that correlate with it](#) over land globally [and study its model dependency](#). We derive seasonal and annual LMR
13 [using a 10-year climatology from multi-year \(2008–2017\) of monthly averaged atmospheric moisture connections at a scale](#)
14 of 0.5° obtained from a Lagrangian atmospheric moisture tracking model. We find that, annually, on average 1.76% ([st.dev. =](#)
15 [1.1%](#)) of evaporated moisture returns as [precipitation rainfall](#) locally, but with large temporal and spatial variability, where
16 LMR peaks in summer and over wet and mountainous regions. ~~We identify~~ [Our results show that](#) wetness, orography, latitude,
17 ~~and~~ ~~ec~~ [convective available potential energy, wind speed, and total cloud cover as drivers of](#) [correlate clearly with](#) LMR,
18 [indicating that especially wet regions with little wind and strong ascending air are favourable for high LMR, indicating a](#)
19 [crucial role for convection](#). [Finally, we find that spatial patterns of local recycling are consistent between different models, yet](#)
20 [the magnitude of recycling varies](#). Our results can be used to study impacts of evaporation changes on local precipitation, with
21 ~~widespread~~ implications for, for example, greening and water management.

22 1 Introduction

23 Atmospheric moisture connections redistribute water from evaporation sources to [precipitation](#) sinks, affecting climates
24 globally, regionally, and locally. These connections are key in the global hydrological cycle and are used to understand the
25 importance of terrestrial evaporation for water availability. [As evaporated moisture can travel up to thousands of kilometres](#)
26 [in the atmosphere, changes in evaporation can affect precipitation in a large area. An evaporation shed](#) (Van der Ent and
27 Savenije, 2013) [describes where evaporated moisture from a specific source region precipitates and therefore, can be used to](#)
28 [study \(1\) the changes in precipitation on a global scale following a change in evaporation in the source region and \(2\)](#)
29 [atmospheric moisture recycling. Globally, more than half of terrestrial evaporated moisture precipitates rains out](#) over land
30 (Van der Ent et al., 2010; Tuinenburg et al., 2020), [which is a process called terrestrial moisture recycling. About half of](#)

31 [terrestrial precipitation originates from land](#) (Tuinenburg et al., 2020). Hence, [terrestrial moisture recycling has an important](#)
32 [contribution to water availability](#). For example, [80% of China's water resources originates from evaporation over Eurasia](#) (Van
33 [der Ent et al., 2010](#)). Furthermore, [areas can also feed precipitation to themselves through regional moisture recycling](#). In the
34 [Amazon basin, 63% of the evaporated moisture precipitates within the basin itself](#) (Tuinenburg et al., 2020). [Terrestrial](#)
35 [moisture recycling is considered an ecosystem service](#) (Falkenmark et al., Wang Erlandsson, & Rockström, 2019; P. W. Keys
36 [et al., Wang Erlandsson, & Gordon, 2016](#)) [as globally, almost 20% of terrestrial precipitation originates from vegetation-](#)
37 [regulated moisture recycling](#) (Patrick W. Keys et al., 2016). [How this ecosystem service is affected by, for instance,](#)
38 [deforestation, can be studied using atmospheric moisture connections](#).

39

40 [Moisture recycling has been used to study downwind impacts of land-use changes](#) (e.g. Bagley et al., 2012; Keys et al., 2012;
41 [Wang-Erlandsson et al., 2018](#)), which can affect both the magnitude and pattern of moisture recycling (Van der Ent et al.,
42 [Wang Erlandsson, Keys, & Savenije, 2014](#)), and the impact of ecosystems on other ecosystems (e.g. O'Connor et al., 2021).
43 [Hence, atmospheric moisture connections can be used for freshwater governance to understand and manage the impacts of](#)
44 [land-use changes downwind such as changes in freshwater availability for irrigation and plants](#). (te Wierik et al. 2021; Te
45 [Wierik et al, 2020](#)). For example, [previous research showed that for 45% of the land surface, an increase in vegetation is](#)
46 [beneficial for downwind water availability](#) (Cui et al., 2022).

47

48 [So far, analytical recycling models and moisture tracking models have been used to study terrestrial recycling and downwind](#)
49 [impacts of land cover change on global and regional levels](#) (Burde & Zangvil, 2001; Van der Ent et al., 2010). Multiple studies
50 [focus on the regional recycling for specific regions, with a spatial scale ranging from 500 km up to several thousands of](#)
51 [kilometres](#) (e.g., Burde, 2006; Dominguez et al., 2006; Lettau et al, 1979; Staal et al., 2018; Trenberth, 1999). Furthermore,
52 [regional recycling on a spatial scale of 1.5° has been studied globally using a Eulerian moisture tracking model, assuming a](#)
53 [well-mixed atmosphere](#) (Van der Ent and Savenije, 2011). [It was debated that regional recycling ratios are difficult to compare](#)
54 [due to differences in the shape and size of the studied regions](#) (Van der Ent and Savenije, 2011). [Therefore, Van der Ent &](#)
55 [Savenije \(2011\) defined the typical length scale of evaporation recycling, which can be used to compare between different](#)
56 [regions because it is independent of the size and shape of a regions](#). This length scale decreases with increasing regional
57 [recycling and, therefore, is a proxy for an area's regional recycling](#). However, it does not allow for the quantification of the
58 [amount of water that recycles within the defined region and therefore does not provide quantitative insight into the regional](#)
59 [impacts of evaporation changes induced by land-cover changes](#).

60

61 [In regions with a high regional recycling, reforestation can enhance freshwater availability and for regions with a low recycling,](#)
62 [reforestation may cause local drying](#) (Hoek van Dijke et al., 2022) due to reductions in streamflow as a result of enhanced
63 [evaporation locally](#) (Brown et al., 2005; Jackson et al., 2005). To physically understand, for instance, the role of local wetting
64 [or drying due to reforestation, deforestation, or the use of groundwater or surface water for irrigation, local moisture recycling](#)

65 [is key. We argue that local impacts need to be studied explicitly as they may have a crucial role in future water governance,](#)
66 [e.g., to prevent tree restoration projects causing local drying.](#)

67
68 [The state-of-the-art high-resolution atmospheric moisture connections obtained with the Lagrangian atmospheric moisture](#)
69 [tracking model “UTrack” allows us to calculate the evaporation recycling ratio at higher spatial resolution \(0.5°\) \(Tuinenburg](#)
70 [et al., 2020; Tuinenburg and Staal, 2020\). We define this as the local moisture recycling ratio \(LMR\) as this high resolution](#)
71 [allows us to study local-scale land-atmosphere feedbacks, which will help us better understand hydrological impacts of land-](#)
72 [use change. LMR describes which fraction of evaporated moisture recycles within its source grid cell and its eight surrounding](#)
73 [grid cells. Moisture recycling has not been studied before on this high-resolution scale globally. To get a better physical](#)
74 [understanding of this metric we identify which factors correlate with it. We analyse this for different latitude classes to account](#)
75 [for different cell sizes across latitude. Factors included in this analysis are: orography, precipitation, precipitation type,](#)
76 [evaporation, shear, convective available potential energy, atmospheric moisture flux, wind speed, total cloud cover, boundary](#)
77 [layer height and surface net solar radiation. These variables relate to either convection, local wetness, or moisture transport](#)
78 [away from the source location, which we identified as important factors for local moisture recycling. Furthermore, we study](#)
79 [how LMR varies over the globe and throughout the year for a 10-year climatology \(2008-2017\), as well as its scaling and](#)
80 [model dependency.](#)

81
82 ~~[We study the relation between local moisture recycling and latitude, orography, precipitation, precipitation type, evaporation,](#)~~
83 ~~[shear, convective available potential energy, and atmospheric moisture flux. These variables relate to either convection, local](#)~~
84 ~~[wetness, or moisture transport away from the source location, which we identified as important factors for local moisture](#)~~
85 ~~[recycling.](#)~~

86 **2 Methods**

87 We use global atmospheric moisture connections obtained from Tuinenburg et al., (2020) to calculate LMR worldwide. These
88 moisture connections are ~~[a 10-year climatology](#)~~~~[multi-yearly](#)~~ (2008–2017) ~~[of](#)~~ monthly averages and have a spatial resolution of
89 0.5°. These UTrack-atmospheric-moisture data are derived using a Lagrangian atmospheric moisture tracking model by
90 Tuinenburg & Staal (2020) ~~[that tracks evaporated moisture at a spatial scale of 0.25°](#)~~. In this model, for each grid cell of 0.25°,
91 each mm of evaporation is represented by one hundred released moisture parcels. The wind transports these parcels
92 horizontally and vertically through the atmosphere. Additionally, a probabilistic scheme describes the vertical movement of
93 the moisture parcels over 25 atmospheric layers. In this scheme, the parcels are randomly distributed across the vertical
94 moisture profile of each grid cell. At each time step (0.1 h), the moisture budget is made using evaporation, precipitation and
95 total precipitable water. Parcels are tracked for up to 30 days or up to the point at which only 1% of their original moisture is
96 still present. ~~[On average, the lifetime of atmospheric moisture is 8-10 days](#)~~ (Sodemann, 2020). ~~[However, some moisture might](#)~~

97 still remain in the parcels after 10 days. After 30 days for most of the parcels all of the original moisture has rained out
 98 (Tuinenburg and Staal, 2020). Input data for UTrack consist of evaporation, precipitation, precipitable water, and wind speed
 99 obtained from the ERA5 dataset (Hersbach et al., 2020). We refer to Tuinenburg & Staal (2020) for a complete description of
 100 the model settings and the tests and assumptions underlying them.

101

102 LMR is the fraction of evaporated moisture that rains out precipitates locally. To study the scale dependency of local moisture
 103 recycling, we examine three definitions of LMR (Fig. A1): the fraction of evaporated moisture that rains out precipitates in f(1)
 104 its source grid cell, i.e., r_1 , (2) its source grid cell and its eight neighbouring grid cells, i.e., r_9 , and (3) its source grid cell and
 105 its 24 neighbouring grid cells, i.e., r_{25} . Equations 1-3 describe the three definitions of LMR, in which $E_{i,j}$ is the amount of
 106 moisture evaporated from source grid cell i,j . The fraction of $E_{i,j}$ that precipitates within its source grid cell and its
 107 (8 or 24) neighbouring grid is indicated by $P_{E,i+l,j+k}$, P is precipitation ($i+l,j+k$, with $l = 0$ and $k = 0$ for r_1 , $l = -1,0,1$ and $k = -$
 108 $1,0,1$ for r_9 and $l = -2,-1,0,1,2$ and $k = -2,-1,0,1,2$ for r_{25}), and i,j the index of the source grid cell and 1 is used to define the
 109 domain i.e. 1, 9 or 25 cells. We calculated seasonal and yearly averages of LMR for our different analyses.

$$110 \quad r_1 = \frac{P_{E,i,j}}{E_{i,j}}$$

111 (1)

$$112 \quad r_9 = \frac{\sum_{l=-1}^1 \sum_{k=-1}^1 P_{E,i+l,j+k}}{E_{i,j}} \quad (2)$$

$$113 \quad r_{25} = \frac{\sum_{l=-2}^2 \sum_{k=-2}^2 P_{E,i+l,j+k}}{E_{i,j}} \quad (3)$$

114

115 r_1 , r_9 , and r_{25} result in different local moisture recycling ratios across the globe (Fig. A2). r_1 peaks over the ocean where
 116 precipitation is relatively low and evaporation is relatively large, which results in relatively large recycling ratios. In addition,
 117 we find exceptionally low values over mountain peaks, yet not over all elevated terrain. This result is inconsistent with the
 118 patterns found for r_9 and r_{25} , as these patterns include peaks over mountainous and low recycling over the oceans. These
 119 patterns can be explained by enhanced convection over mountains due to orographic lift and strong winds over the ocean that
 120 carry moisture away from its source. The patterns found for r_9 and r_{25} seem to capture multiple physical processes that are
 121 important for moisture transport and formation of precipitation better than the pattern of r_1 . In our study we do not focus on r_1 ,
 122 as r_1 does not include all small-scale flows of <50 km. This is because moisture can evaporate from cell i,j , and precipitate in
 123 the adjacent cell, while transport length is <50 km. Furthermore, as the patterns of r_9 and r_{25} are similar and agree with our
 124 understanding of relevant processes, we decided to define the local moisture recycling ratio (LMR) as r_9 to keep the spatial
 125 scale as small as possible. For r_9 , the distance from the center of the source grid cell and its surrounding grid cells describes
 126 the typical length of the local moisture flow. We calculated this typical length across the globe by calculating the average of
 127 the average zonal length, meridional length, and diagonal length of all terrestrial grid cells. The total average equals 50.1 km
 128 (st.dev. = 15.5 km), so, the average moisture flow length is approximately 50 km.

130 Furthermore, the LMR derived with the Lagrangian approach using output from UTrack is compared with the output from the
 131 Eulerian moisture tracking model WAM2-layers (Link et al., 2020), to study the model dependency of LMR. For this
 132 comparison, the resolution of the UTrack data is reduced to 1.5° to match the output of the WAM2-layers model. To do so, all
 133 evaporationsheds over land were multiplied with their source evaporation. Then, the recycling within cells of 1.5° was
 134 calculated for all terrestrial surfaces. A detailed description of the atmospheric moisture connections obtained with WAM2-
 135 layers and the model itself are provided by Link et al. (2020) and Van der Ent et al. (2013).

136

137 We study the relations between multiple variables and the 10-year climatology (2008-2017) of local moisture recycling to
 138 identify drivers-factors that affect recycling. To calculate this 10-year climatology of LMR, for each month, we weighted
 139 the multi-year (2008-2017) monthly LMR by multi-year monthly evaporation in the same period:

$$140 \quad LMR_{annual\ average} = \sum_{dec}^{i=jan} LMR \frac{E_{month\ i}}{E_{year}} \quad (4)$$

141 in which E_{year} is the sum of the evaporation of the 12 months. To identify these factors that affect LMR, drivers-are-variables
 142 that relate to atmospheric moisture and vertical displacement of air, as both higher atmospheric moisture content and ascending
 143 air promote rainfall-precipitation are selected. All these variables are obtained, either directly or indirectly from ERA5
 144 reanalysis data (Hersbach et al., 2020). We downscaled the original resolution from 0.25° to 0.5° by centrally averaging the
 145 data.

146

147 The variables that we In total 13 variables are selected (Fig. A3) assessed are: (1) elevation (z) which we expect to enhance
 148 LMR through orographic lift. (2) Precipitation-precipitation (P), which we expect to correlate positively with LMR given that
 149 in Lagrangian moisture tracking models, the amount of moisture that leaves the parcel (i.e., precipitates) scales with
 150 precipitation. (3) Total evaporation evaporation (E) as it enhances the atmospheric moisture content and we, therefore, expect
 151 it to promote precipitation locally. (4) Wetness (P precipitation minus evaporation- E), as with increasing wetness the
 152 downward flux of moisture increases and evaporated water becomes more likely to precipitate, possibly promoting LMR. (4)
 153 Convective precipitation (cp) and fraction of convective precipitation, (5) large-scale precipitation (lsp), as they scale with
 154 precipitation, by definition. Both are included to study whether the type of precipitation is an important factor explaining LMR.
 155 fraction of large-scale precipitation, (6) Latitude, which is a proxy for processes related to the Hadley cell circulation, which
 156 is characterized by strong ascent and descent of air at specific latitudes, which we expect to have an important contribution to
 157 LMR, because they respectively enhance and reduce the formation of precipitation (Wang and Yang, 2022). (7) The vertical
 158 integral of the atmospheric moisture flux (in northward and eastward directions and the total flux) as it carries the moisture
 159 away from its source and could thus reduce LMR. (8) Convective available potential energy ($CAPE$), which feeds convection
 160 and therefore promotes precipitation locally, which could enhance LMR. (9) Vertical wind shear between 650 and 750
 161 hPa of both meridional and zonal winds, as it affects moisture transport in multiple directions and, therefore, we expect it to

162 [impact LMR. \(10\) Total wind speed, as it carries the wind, and therefore, we expect it to correlate negatively with LMR. \(11\)](#)
163 [Total cloud cover as a proxy for condensation processes which possibly enhance LMR \(Richards and Arkin, 1998\). \(12\)](#)
164 [Boundary layer height, because thinner boundaries need less evaporation to reach saturation of air, and therefore, we expect it](#)
165 [will promote precipitation locally. Finally, \(13\) net surface solar radiation as a proxy for the energy source of convection, and](#)
166 [other processes, which we expect to be important for LMR.](#) We calculate shear (τ) using Equation (5).

$$167 \tau = \frac{\ln \frac{v_2}{v_1}}{\ln \frac{z_2}{z_1}} \quad (5)$$

168 In this equation, v_1 and v_2 are the wind speed ([in zonal and meridional directions](#)) at two different heights (z_1 and z_2). We
169 identified significant ~~relations~~ [correlations](#) using Spearman rank correlations. [It should be noted that a correlation does not](#)
170 [imply causality. We exclude oceans, seas and Antarctica from this analysis using the land-sea mask from ERA5. We classify](#)
171 [the data based on latitude to account for decreasing grid cell size with increasing latitude. Each class has a range of 15° and](#)
172 [includes the grid cells on both the Northern and Southern Hemispheres \(see Table A1\). Between 60° and 90° south, the grid](#)
173 [cells do not contain land besides Antarctica, and are therefore not included in the classes.](#) Additionally, we used the Ecoregions
174 2017 data (<https://ecoregions.appspot.com/>) to study the spatially averaged local moisture recycling of 14 biomes across the
175 globe (Fig. A24). We study variation amongst biomes, as biomes include information [on both biotic factors such as vegetation](#)
176 [type,](#) and abiotic factors such as climate.

177 3 Results

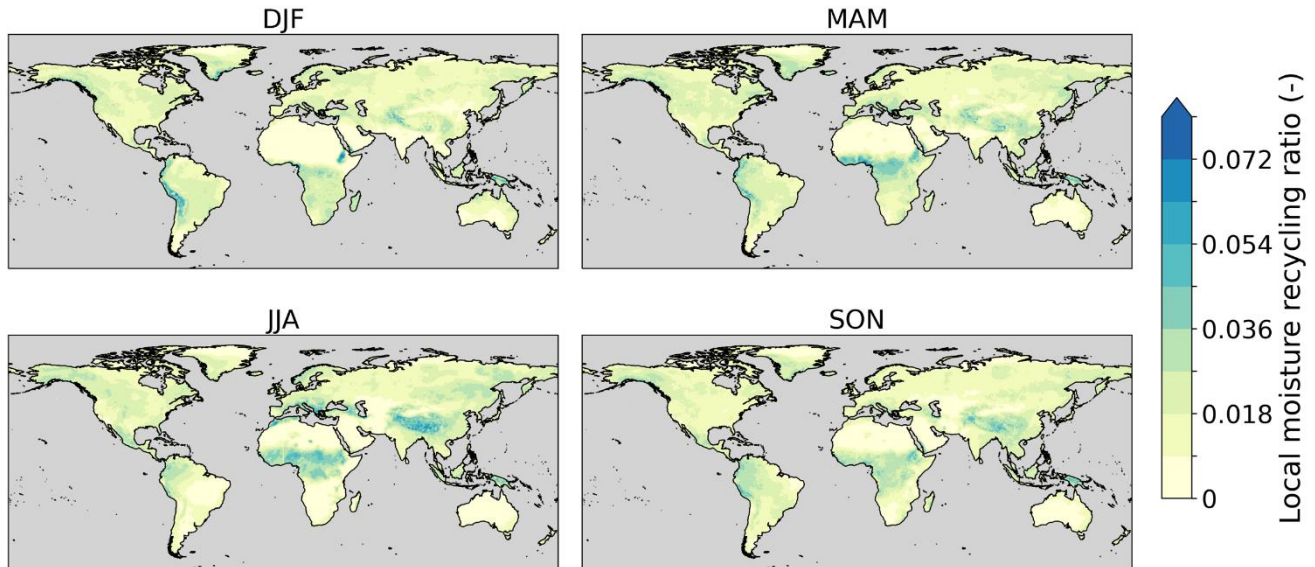
178 3.1 LMR obtained from output of UTrack

179 ~~We find differences across the globe for the three different definitions of local moisture recycling (r_1 , r_9 and r_{25}) (Fig.~~
180 ~~A3). For r_1 , we find maxima over the oceans in areas where precipitation is relatively low, unlike evaporation (Fig. A5),~~
181 ~~which results in relatively high recycling ratios (Fig. A3). However, for r_9 and r_{25} we find maxima over land suggesting~~
182 ~~recycling over nine and 25 grid cells better captures relatively large moisture transport over the oceans than recycling~~
183 ~~over one grid cell does. Furthermore, for r_1 , we find low values over elevated areas (e.g., the Andes mountains)~~
184 ~~compared to r_9 and r_{25} , which show maxima over elevated regions. Hence, there is no clear relation between r_1 and~~
185 ~~either r_9 or r_{25} . These results seem to indicate that the tracking method we use is not sufficient to define recycling within~~
186 ~~one grid cell. Finally, scaling recycling to the number of grid cells, we find r_9 and r_{25} do not relate linearly. For lower~~
187 ~~recycling, r_9 exceeds r_{25} and for higher recycling, r_{25} exceeds r_9 (Fig. A3). In the following, we define local moisture~~
188 ~~recycling (LMR) as r_9 to keep the spatial scale as small as possible but to still have a spatial pattern that we can explain~~
189 ~~physically.~~

190

191 Annually, on average about 1.76% ([st. dev. = 1.1%](#)) of terrestrial evaporated moisture recycles locally. LMR shows spatio-
192 temporal variation (Fig. 1) with peaks over elevated (e.g., the Atlas Mountains and Ethiopian Highlands) and wet areas (e.g.,
193 Congo Basin and Southeast Asia) and minima over arid regions (e.g., Australia and the Sahara Desert). Additionally, we find
194 peaks in LMR during summer (i.e., during DJF for the Southern Hemisphere and during JJA for the Northern Hemisphere).

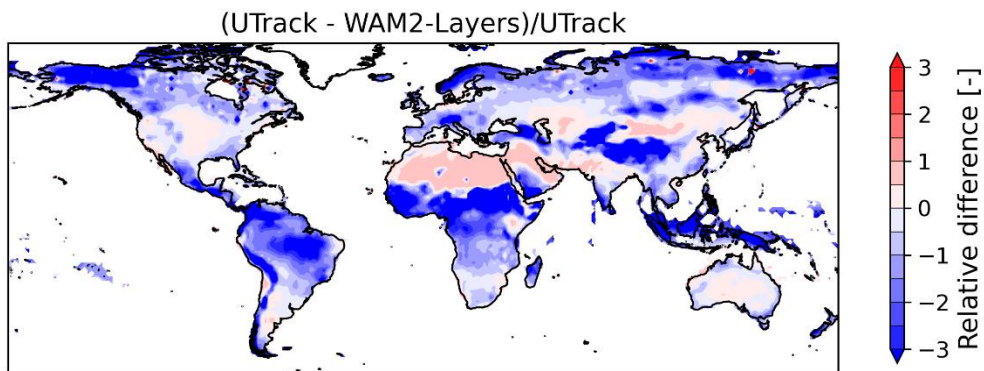
195 This seasonality is especially strong over mountainous and wet areas. For the mid-latitudes, especially the Mediterranean Basin
 196 shows seasonality with peaks in summer (JJA). However, sSeasonality is largest at low latitudes. Within the tropics we find
 197 some spatial differences. First, LMR in the Congo Basin and Southeast Asia exceed LMR in the Amazon Basin. Second,
 198 recycling in the Congo Basin and Southeast Asia peaks in JJA and recycling in the Amazon Basin peaks in DJF, which is thea
 199 wet season for a large part of the Amazon.



200
201

202 **Figure 1. Multi-year 10-year climatology (2008–2017) of the** seasonal averages of local moisture recycling across the global land
 203 surface. Here, local moisture recycling is defined as the fraction of evaporated moisture that ~~rains out~~ precipitates in its source grid
 204 cell and its eight neighbouring grid cells (r_9). Different seasons are DJF: December–February, MAM: March–May, JJA: June–
 205 August, and SON: September–November.

206 We calculated recycling on a 1.5° grid using both the dataset by (Link et al., (2020), which we refer to as $r_{WAM2-layers}$, and the
 207 dataset by (Tuinenburg et al., (2020) (upscaled to 1.5°), which we refer to as r_{UTrack} , to study the model dependency of local
 208 recycling. We find that the global spatial patterns of r_{UTrack} and $r_{WAM2-layers}$ agree (Fig. 2 & Fig. A5). However, the magnitude
 209 of $r_{WAM2-layers}$ is larger than r_{UTrack} over mountains, the tropics, and the high latitudes. r_{UTrack} is larger than $r_{WAM2-layers}$ over
 210 drylands and deserts (e.g., the Sahel region and Western Asia) (Fig. 2). Globally, the difference between r_{UTrack} and $r_{WAM2-layers}$
 211 and its variation is largest around the equator (Fig. A6). On average, the relative difference between UTrack and WAM2-
 212 Layers $((UTrack - WAM2-Layers) / UTrack)$ equals -1.5 (st.dev. = 3.4).



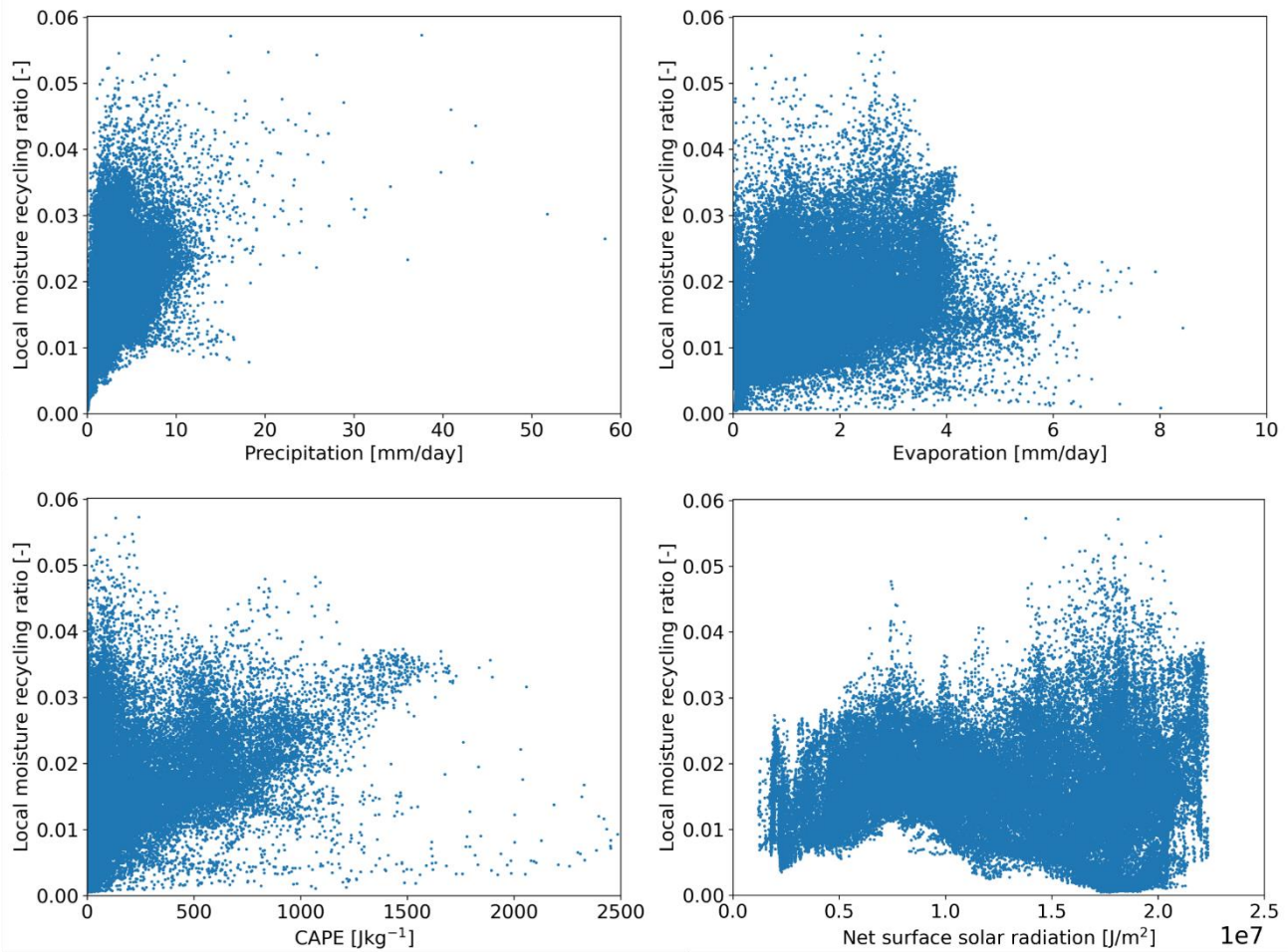
213

214 **Figure 2. The relative deviation between r_{Utrack} and $r_{WAM2-layers}$. This deviation is calculated using the recycling within one grid cell at**
 215 **a resolution of 1.5° obtained from the datasets of (Tuinenburg et al., (2020) and (Link et al., (2020).**

216 **3.2 Factors underlying LMR**

217 For each latitude class we calculated the Spearman rank correlation coefficient (ρ) (Table 1). Below we discuss only
 218 statistically significant ($p < 0.05$) correlations with $\rho \geq 0.4$, indicating a moderate correlation. These correlations are emboldened
 219 in Table 1. We find that LMR correlates positively with total precipitation (tP) and wetness (P-E) for all classes between 15°
 220 and 75° . In addition, between 15° and 30° , LMR correlates strongly with tP ($\rho = 0.80$). Furthermore, large scale precipitation
 221 (between 15° and 45° and between 60° and 75°) and convective precipitation (between 15° and 45°) correlate positively with
 222 LMR. The highest correlation between LMR and convective precipitation is found between 15° and 30° latitude. Here LMR
 223 also correlates positively with evaporation and CAPE, which enhances convective precipitation. Despite the low correlation
 224 between LMR and CAPE for most of the latitude classes, high CAPE clearly relates to LMR, as the skewed profile in the
 225 scatter density plot indicates that only a small amount of the grid cells with a relatively high CAPE have a low LMR (Fig 3).
 226 Furthermore, the presence of clouds also correlates with LMR. Between LMR and total cloud cover, a positive correlation
 227 holds between 15° and 45° , and a negative correlation holds between 60° and 75° . The vertical integral of the eastward and
 228 northward moisture fluxes correlate less with LMR compared to vertical fluxes (e.g., precipitation) as for the higher latitudes,
 229 the northward moisture flux correlates positively with LMR (between 60° and 75°) and the eastward moisture flux correlates
 230 negatively with LMR (between 75° and 90°). However, wind speed correlates negatively with LMR for the lower latitudes
 231 (between 0° and 45°). Furthermore, LMR correlates positively with orography between 30° and 75° . We find that for high
 232 elevation, LMR is always relatively high (Fig A7). Additionally, LMR correlates negatively with boundary layer height
 233 between 45° and 60° . Finally, LMR correlates negatively with shear at 650 hpa in the meridional direction (between 75° and
 234 90°) and latitude (between 60° and 75°). However, we find an oscillating relation between LMR and latitude (Fig 4), which is
 235 not captured by the Spearman rank correlation coefficients. This pattern indicates high values of LMR over the equator (0°)
 236 and 60° north, and low values around 30° north and south. Orography seems to disrupt the relation between latitude and LMR
 237 causing peaks in LMR around 35° north and 20° south (Fig 4). LMR does not correlate to surface net solar radiation for any

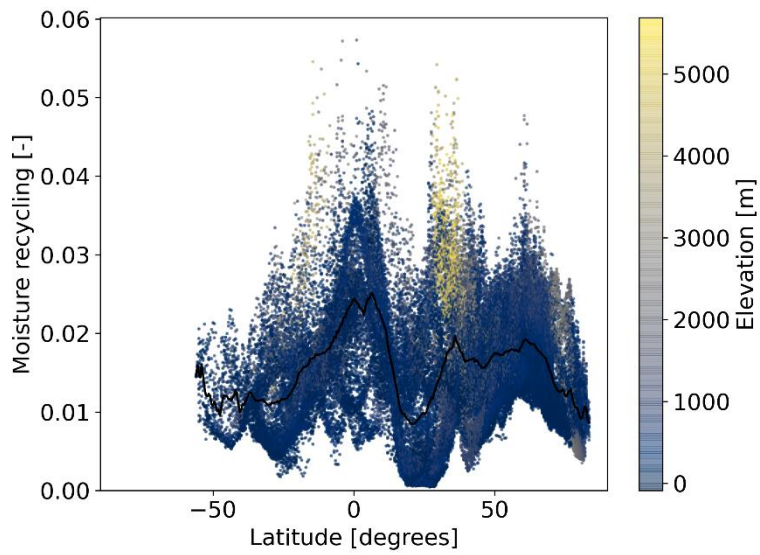
238 [latitude](#). However, for low surface net solar radiation ($<0.75 \cdot 10^6 \text{ J/m}^2$) holds that LMR increases with increasing surface net
239 [solar radiation](#) (Fig 3).



240
241 **Figure 32:** Scatter plots of ~~multi-year~~the 10-year climatology (2008–2017) of the ~~annual averages of~~local moisture recycling ratio
242 over land and precipitation (top left), evaporation (top right), convective available potential energy (CAPE) (bottom left), and
243 ~~latitude~~solar net surface radiation (bottom right). Each dot represents a 0.5° resolution grid cell over land. For the latter the
244 ~~colour scale indicates elevation, with blue being low elevation and yellow being high elevation, and a black line is plotted to show the~~
245 ~~zonal average of local moisture recycling over land at 0.5° resolution.~~

246

247



248

249 Figure 4. Scatter plot of the 10-year climatology (2008-2017) of LMR and latitude. The colour scale indicates elevation, with blue
250 being low elevation and yellow being high elevation. The black line represents the zonal average of LMR. Each dot represents a
251 0.5° resolution grid cell over land.

252

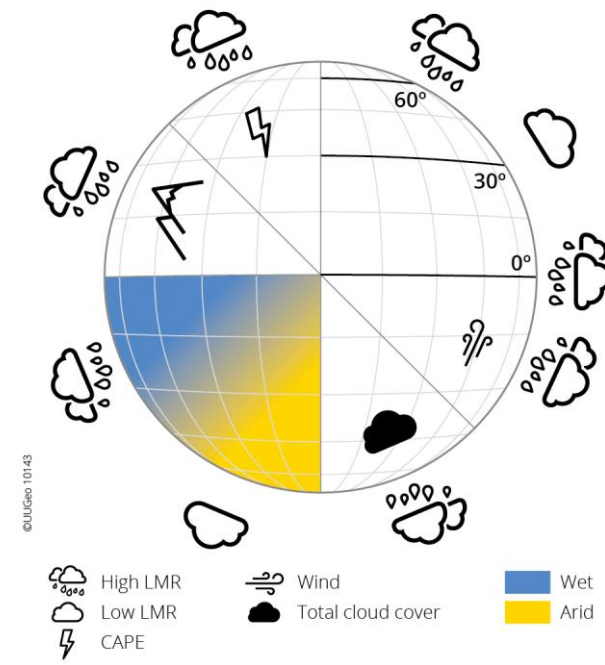
253 **Table 11.** Spearman rank correlation coefficients between LMR and all tested variables. “*” indicates a significant correlation
 254 ($p < 0.05$) and moderate and strong relations ($\rho > 0.4$) are emboldened. The classes including latitudes between 0° and 60° include grid
 255 cells of the Northern Hemisphere and Southern Hemisphere. The classes including latitudes exceeding 60° include grid cells of the
 256 Northern Hemisphere only.

Variable	Spearman rank correlation coefficient					
	$0^\circ-15^\circ$	$15^\circ-30^\circ$	$30^\circ-45^\circ$	$45^\circ-60^\circ$	$60^\circ-75^\circ$	$75^\circ-90^\circ$
Total precipitation (P_{tot})	0.415* 3*	0.80*	0.47*	0.40*	0.45*	0.37*
Total evaporation (E)	-0.05*	0.63*	0.19*	-0.12*	0.19*	0.20*
Wetness (P-E)	0.18*	0.59*	0.52*	0.48*	0.43*	0.27*
Convective precipitation (e_p)	0.20*	0.79*	0.46*	0.29*	0.35*	0.33*
Large scale precipitation (s_p)	-0.06*	0.75*	0.46*	0.38*	0.40*	0.36*
e_p/s_p	0.36*	-0.35*	-0.13*	-0.14*	0.19*	0.28*
Fraction of e_p	0.36*	-0.35*	-0.13*	-0.14*	0.19*	0.28*
Fraction of s_p	0.36*	-0.35*	-0.13*	-0.14*	0.19*	0.28*
Latitude	0.24*	-0.18*	0.22*	0.14*	-0.40*	-0.18*
Eastward moisture flux	0.15*	0.00	-0.30*	-0.38*	-0.20*	-0.49*
Northward moisture flux	-0.03*	0.22*	0.29*	-0.03*	0.48*	0.23*
Total moisture flux	-0.28*	0.30*	-0.29*	-0.33*	-0.03	-0.16*
CAPE	0.31*	0.58*	0.37*	0.06*	0.12*	-0.02
Zonal shear	0.15*	-0.12*	0.02	-0.31*	0.00	0.24* 5
Meridional shear	-0.22*	0.15*	-0.08*	-0.01	0.05*	-0.46*
Orography	0.31*	0.29*	0.49*	0.54*	0.68*	-0.13*
Total cloud cover	0.28*	0.78*	0.43*	0.09*	-0.56*	0.08*
Surface net solar radiation	-0.16*	0.10*	-0.30*	-0.08*	0.28*	0.21*
Boundary layer height	-0.31*	-0.32*	-0.39*	-0.53*	-0.18*	-0.06*
Total wind speed	-0.46*	-0.55*	-0.47*	-0.26*	-0.26*	-0.30*

257 **4 Discussion**

258 **4.1 Factors underlying LMR**

259 Moisture recycling affects humanity by influencing water security, agriculture, forestry, regional climate stability and Earth
260 system resilience (Keys et al., 2019; Wang-Erlandsson et al., 2022). Different types of moisture recycling were subject to
261 research used for different applications (e.g., Bagley et al., 2012; Pranindita et al., 2022; Van der Ent et al., 2010), but for the
262 first time, we analysed the local moisture recycling ratio (LMR) (of evaporated moisture) and its drivers across the globe at
263 0.5° resolution, and which factors affect it. We find that LMR, defined as the fraction of evaporated moisture that rains
264 outprecipitates within a distance of 0.5° (typically 50 km) from its sourceapproximately 50 km of its source location, varies
265 over time and space, peaking in summer and over elevated and wet regions. First, we identified latitude, elevation, and
266 Convective Available Potential Energy (CAPE) as important drivers-factors influencingof LMR (Fig. 53). These variables all
267 promote convection (Roe, 2005; Scheff and Frierson, 2012; Wallace and Hobbs, 2006), strongly suggesting a dependencye of
268 LMR on convection. Convective storms develop due to unstable conditions resulting in precipitation locally (Eltahir, 1998)
269 and a higher CAPE results in more rainfall (Eltahir and Pal, 1996; Williams and Renno, 1993). The pattern of LMR across
270 latitudes also coincides with updraft and downdraft of air caused by the Hadley cell circulation (Wallace and Hobbs, 2006).
271 Around the equator and 60° north and south, air ascends, whereand we find a high LMR. Additionally, air descends aA
272 30° north and south, air descends, where we find a low LMR. Deviations from this pattern correspond to higher elevations
273 which promotepromoting LMR through orographic lift. Overall, our results suggest a positive relation between convection and
274 LMR.



275

276 **Figure 53. Conceptual model of the most important drivers-factors influencing local moisture recycling around the globe. Rainy**
277 **clouds indicate variables that increase LMR and clouds without raindrops indicate variables that decrease LMR. Blue indicates wet**
278 **regions, yellow indicates arid regions.**

279 Second, we find that wetness is an important ~~factor underlying driver of~~ LMR as LMR significantly correlates with precipitation
280 (P) and $P-E$ (precipitation minus evaporation). Furthermore, both large-scale and convective precipitation significantly
281 correlate with LMR. This is surprising, as convection promotes precipitation locally (Eltahir, 1998); therefore, we expected a
282 stronger correlation between LMR and convective precipitation than between LMR and large-scale precipitation. As both
283 correlations are similar, this suggests that the type of precipitation does not affect LMR. Although convection is a local-
284 scale process (i.e., having a spatial scale of below 100 km) (Miyamoto et al., 2013), remotely evaporated moisture can be
285 transported to a region with high convective activity and then ~~rains out~~precipitate as convective precipitation (Jana et al.,
286 Rajagopalan, Alexander, & Ray, 2018; Liberato et al., 2012). In that way, the precipitation type is independent of the distance
287 between moisture source and target location and therefore does not relate to LMR. Total cloud cover correlates both positively
288 (between 15° and 45°) and negatively (between 60° and 75°) with LMR. Total cloud cover correlates with precipitation,
289 convective precipitation, and large-scale precipitation for all latitudes except between 60° and 75° (Tab. A2). Due to the
290 positive correlation between LMR and precipitation and the absence of a correlation between precipitation and total cloud
291 cover at these latitudes we can statistically explain the negative correlation between total cloud cover and LMR. Physically,
292 this result is harder to explain. Our results describe the importance of convection underlying LMR at lower latitudes, where
293 total cloud cover correlates with convective precipitation. For higher latitudes, the importance of convection underlying LMR
294 decreases, and we therefore expected also the correlation between total cloud cover and LMR to decrease but not to become
295 negative. Likely, another process that we cannot identify with our analysis causes the correlation between total cloud cover
296 and LMR to be negative. Overall, we find that wetness enhances LMR independent of the precipitation type.

297
298 ~~However, a~~Unexpectedly, we do not ~~find~~identify a ~~relation~~clear correlation between the vertical integral of the atmospheric
299 moisture flux and LMR. However, for the lower latitudes (between 0° and 45° latitude), LMR correlates to wind speed (at 10
300 and 100 m) which carries evaporated moisture away from its source location, enhancing the moisture flux. Therefore,
301 horizontal moisture fluxes at specific altitudes are better for our analysis than the vertical integral of the moisture flux.
302 However, since wind carries moisture away from its source, we expected that wind speed and LMR would also correlate for
303 the higher latitudes (latitude above 45°). It could be that for the higher latitudes, a more significant amount of moisture is
304 present at higher latitudes, explaining why LMR and wind at 10m do not correlate. However, wind speeds at 650 hpa and 750
305 hpa also do not correlate to LMR for these latitudes (Tab. A2). ~~Overall, we find that wetness enhances LMR independent of~~
306 the precipitation type.

307
308 Despite the importance of vertical shear in atmospheric moisture tracking models (Van der Ent et al., 2013), we do not find a
309 correlation between local moisture recycling and vertical shear between 650 and 750 hPa. Shear is the friction between air

310 layers that minimizes complete mixing, which for some regions around the world is strongest between 650 and 750 hPa
311 (Dominguez et al., 2016). A possible explanation is that due to its small spatial scale, the temporal scale of LMR is also small,
312 which may prevent the air reaching 700 hPa within the spatial scale of LMR. Furthermore, it is possible that our study design
313 is insufficient to capture the relation between LMR and shear throughout the year over the globe. We aimed for a general
314 analysis to identify the main factors that influence LMR. A more detailed study that distinguishes between different seasons
315 and isolates different climate zones is necessary to identify more factors that influence LMR as some factors might be more
316 important during a specific season. For example, convection occurs more during summer than during winter, and therefore,
317 might have a stronger correlation with LMR during summer. Besides, some factors are shape and size dependent similar to
318 LMR, while other factors are not dependent on grid cell size and shape. This might cause bias in the results of the Spearman
319 analysis. Furthermore, due to the many interactions within the Earth system and, consequently, between the variables included
320 in our study, it is impossible to determine the true drivers of LMR. However, the correlations do indicate how changes in the
321 environment might affect LMR.

322 4.2 regional patterns

323

324 To zoom in on the importance of each of the different drivers of factors underlying LMR for various areas across the globe,
325 we determined LMR for the major global biomes (Fig. A78). LMR is highest for the wet tropics (between 0° and 15° north
326 and south) and montane grasslands and lowest for desert-like biomes in both the Northern and Southern Hemisphere (between
327 30° and 45° north and south), confirming the importance of wetness, orography, and latitude. However, in the tropics (between
328 0° and 15° latitude), we do not find any correlation between LMR and precipitation, evaporation, wetness, or orography.
329 Possibly, due to the abundance of water and energy to evaporate, there is LMR under all circumstances, except for when the
330 wind speed is high. However, Comparing LMR for each biome differences between both hemispheres indicate s that some of
331 the ~~drivers~~ factors underlying LMR are more robust than other ones ones for some biomes. In the Mediterranean biomes,
332 located between 30–40° north and south, air generally descends due to the Hadley cell circulation. As a result, these biomes
333 are expected to have low LMR. Although we find a low LMR for the Mediterranean biomes in the Southern Hemisphere, we
334 find a relatively high LMR for the Mediterranean biomes in the Northern Hemisphere. The Spearman rank analysis indicates
335 that at these latitudes, wind speed correlates with LMR, which may explain the difference between both hemispheres. This is a
336 surprising result, which does not overlap with the different Mediterranean climate subclasses (i.e., hot summer Mediterranean
337 climate and warm summer Mediterranean climate)(Peel et al., 2007). More research is needed to understand this difference
338 better.

339

340

341 Although LMR is the highest in the wet tropics, we find different results among the various tropical regions (Amazon Basin,
342 Congo Basin & Southeast Asia). LMR in the Congo Basin exceeds LMR in the Amazon Basin (Fig. 1), despite larger amounts
343 of rainfall-precipitation in the Amazon Basin (Hersbach et al., 2020). In the tropics, current deforestation results in drying
344 (Bagley et al., 2014; Staal et al., 2020), reducing evaporation. For the Amazon Basin, drought is related to higher deforestation
345 rates (Staal et al., 2020). As LMR in the Congo Basin exceeds LMR in the Amazon Basin, deforestation has a relatively large
346 impact on local precipitation in the Congo Basin, suggesting a larger impact~~higher impact~~ on droughts ~~and deforestation~~
347 locally. This is further exacerbated by the fact that the Congo Basin, in comparison with the Amazon Basin, has many small-
348 scale moisture feedback loops. (Wunderling et al., ~~Wolf, Tuinenburg, & Staal, 2022~~). ~~The latter is true when assuming drought~~
349 ~~also enhances deforestation in the Congo Basin.~~ Unlike LMR, basin recycling is similar for both basins (Tuinenburg et al.,
350 2020). Suggesting~~Thus~~, the impact of deforestation on precipitation in the entire basin is similar for both basins, indicating
351 both basins would experience similar overall drying. However, drought conditions can also enhance recycling ratios (Bagley
352 et al., 2014), ~~thus possibly~~ promoting LMR. Further research is necessary to understand the impact of deforestation on LMR
353 in the tropics in more detail.

354 4.3 The spatial scale of the local moisture recycling ratio

355 We study local moisture recycling on a spatial scale of 0.5°, which is approximately 55 km around the equator and 50 km on
356 average globally for all land cells. Instead of recycling within one grid cell (r_1), we studied the recycling of evaporated moisture
357 within its source grid cell and its 8 surrounding grid cells. Compared to r_1 , this r_9 includes all moisture flows with a length
358 scale of typically 50 km. For r_1 , moisture flows with a length smaller than 50 km can occur close to the border of grid cells
359 and therefore, r_1 by definition underestimates the actual recycling. These moisture flows are accounted for in r_9 .

360
361 However, defining LMR on a grid scale gives complications. First, the longitudinal distance for a grid cell size decreases with
362 latitude, resulting in different sizes and shapes, which makes it difficult to compare LMR among all grid cells. For the low-
363 and mid-latitudes, the variation in grid cell size affects LMR only slightly, as confirmed when LMR for each grid cell was
364 scaled to a single area (Fig. A9). Therefore, we believe that the variation in grid size causes only a small bias in the statistical
365 analysis, as the largest fraction of the land surface is at the low- and mid-latitudes, and moisture recycling is less important for
366 the higher latitudes. However, it should be noted that for similar wind speed, LMR will be lower in smaller grid cells than
367 larger grid cells. Second, the spatial scale of recycling is strongly dependent on regional differences such as biome type, the
368 dominating winds, and the proximity to mountains. For instance, with increasing distance to the Andes mountains the median
369 travelling distance of transpired moisture from the Amazon forest increases (Staal et al., 2018) and for the Ganges basin,
370 evaporated moisture is blocked by the Himalayas, limiting upward moisture flow and inducing precipitation (Tuinenburg et
371 al., ~~Hutjes, & Kabat, 2012~~). Further, precipitation can be triggered by micrometeorological processes (e.g. (Knox et al., ~~Bisht,~~
372 Wang, & Bras, 2011; Taylor et al., ~~de Jeu, Guichard, Harris, & Dorigo, 2012)~~ making it unknown at what spatial scale moisture
373 recycling is the dominant process for precipitation. Therefore, we believe that a grid-based approach to systematically study

374 [LMR globally is a solid approach to define and study the physical processes at a spatial scale >50 km through, for instance,](#)
375 [the Spearman analysis to study the underlying processes. However, our definition of LMR is not sufficient to identify processes](#)
376 [on a spatial scale smaller than 50 km that might be relevant.](#)

377 [4.4 Model and definition dependencies](#)

378 [It is important to note that the typical length scale of moisture recycling, as defined by Van der Ent & Savenije \(2011\), allows](#)
379 [for a comparison of regional moisture recycling for different regions around the world due to its independence of the region's](#)
380 [size and shape \(Fig A10\). The typical length scale of evaporated moisture recycling decreases with increasing recycling. It](#)
381 [peaks over deserts and is small over the tropics and mountainous regions \(Fig A9\), overlapping with the spatial pattern of](#)
382 [LMR. The spatial patterns of LMR, obtained in our study, resemble the spatial patterns of the regional recycling ratio \(LMR is](#)
383 [smaller than regional recycling\) obtained by Van der Ent & Savenije \(2011\), who estimated average regional recycling ratios](#)
384 [within a 1.5° grid cells globally between 1999 and 2008, using a Eulerian moisture tracking model. Due to different model set-](#)
385 [up and grid cell sizes, differences in the magnitude of recycling are expected; hence, here we only look at the qualitative](#)
386 [patterns.](#)

387 [However, this typical length scale does not allow for the quantification of the amount of recycled moisture and therefore, it is](#)
388 [difficult to apply this metric to study the impact of evaporation changes due to land-use change. Therefore, studies that aim to](#)
389 [quantify moisture recycling locally may best use recycling ratios. However, studies that aim to compare recycling among](#)
390 [different regions can best use the typical length scale of recycling.](#)

391
392 [In this article, we focus on model dependency as we calculated the differences in magnitude of recycling within one grid cell](#)
393 [of 1.5° obtained from output of the UTrack and WAM2-layers models \(Link et al., 2020; Tuinenburg et al., 2020\). The spatial](#)
394 [patterns are similar, yet the different magnitudes indicate a large model dependency, and, therefore, an uncertainty in moisture](#)
395 [recycling. Furthermore, Van der Ent et al. \(2010\) calculated recycling within a grid cell of 1.5° for the years 1999–2008 using](#)
396 [WAM2-layers and found a similar spatial pattern with high recycling over mountainous and tropical regions and low recycling](#)
397 [over desert-like regions. These recycling ratios also have a larger magnitude than LMR. However, it is not straightforward to](#)
398 [interpret the differences in recycling ratios as both models use different input data \(i.e., ERA5 and ERA-Interim\). To assess](#)
399 [the possible role of the models in causing the difference in moisture recycling, we describe the main differences between the](#)
400 [models. First, WAM2-layers calculates the atmospheric moisture recycling on a larger temporal and spatial scale than UTrack,](#)
401 [A larger grid cell size and time step increases the likelihood of evaporation and precipitation taking place within the same](#)
402 [small amount of time, which might result in an overestimation of recycling within one grid cell. Second, WAM2-layers](#)
403 [generates moisture flows using two vertical layers; therefore, strong winds at specific vertical levels will be described in less](#)
404 [detail, reducing estimated moisture transport and enhancing estimated moisture recycling within a single grid cell. Differences](#)
405 [between \$r_{UTrack}\$ and \$r_{WAM2-layers}\$ are highly visible over mountainous regions where wind experiences relatively strong friction,](#)
406 [highly impacting the wind. Finally, different approaches are used to include vertical mixing in the two models. Vertical mixing](#)

407 [causes the greatest error in moisture tracking models, but it is unknown to what extent vertical mixing is underestimated](#) (Stohl
408 [et al., Forster, Frank, Seibert, & Wotawa, 2005; Tuinenburg & Staal, 2020](#)).

409

410 Besides [studies using](#) atmospheric moisture tracking (e.g., Bagley et al., 2014; Keys et al., 2014; Van der Ent et al., 2010),
411 [some](#) previous studies used different methods to calculate regional moisture recycling for a specific area, such as isotope
412 measurements (e.g., An et al., 2017) and [bulk](#) recycling models (e.g., Burde & Zangvil, 2001). The most common recycling
413 models are modifications of Budyko's model (Budyko, 1974; Burde and Zangvil, 2001), which are 1D or 2D analytical models.
414 These models assume that the atmosphere is completely mixed, meaning that evaporated water directly mixes perfectly with
415 advected water throughout the entire water column. Because of this assumption, first, these models overlook fast recycling,
416 which describes local showers that yield [rain-precipitation](#) before the evaporated water is fully mixed. [Excluding fast recycling](#)
417 [causes models to underestimate terrestrial moisture recycling for some regions \(e.g., Amazon Basin\)](#) (Burde et al., 2006b).
418 Second, these models ignore the influence of vertical shear, which causes a significant error (Dominguez et al., 2020).
419 ~~[Excluding fast recycling causes models to underestimate terrestrial moisture recycling for some regions \(e.g., Amazon Basin\)](#)~~
420 ~~[\(Burde et al., 2006b\). To obtain LMR, evaporated moisture is tracked through the atmosphere with a Lagrangian model in](#)~~
421 ~~[three spatial dimensions](#)~~. Our method minimizes the errors due to fast recycling and vertical shear because of two model
422 aspects. First, at each time step, each parcel has a small chance of getting mixed, causing each parcel to move approximately
423 once in the vertical direction every 24 hours, ~~[besides additional to](#)~~ the displacement [based on reanalysis data of](#) ~~[caused by](#)~~
424 ~~[vertical winds](#)~~. ~~[As parcels are released from the surface,](#)~~ [T](#)his process minimizes complete mixing and reduces the error due
425 to shear and fast recycling. Second, the error due to fast recycling also becomes smaller because lower atmospheric levels
426 contribute more to the total precipitation than higher levels due to the skewed vertical moisture profile. [WAM2-layers accounts](#)
427 [for vertical shear as it models two vertical atmospheric layers of which the interface is located at the height at which shear](#)
428 [typically occurs. These two layers are both completely mixed and therefore, compared to bulk models, WAM2-layers better](#)
429 [represents the distribution of moisture throughout the atmospheric column. As an alternative method, moisture flows can be](#)
430 [calculated on a smaller time step to increase the interactions between different wind components, resulting in a better](#)
431 [representation of turbulence](#) (Keune et al., Schumacher, & Miralles, 2022). Despite the error reduction, the representation of
432 fast recycling in UTrack should be studied in more detail, as fast recycling is expected to influence LMR significantly.

433

434 [LMR is calculated as a ten-year average. This period of ten years might miss multi-year climate variability such as the El Niño](#)
435 [Southern Oscillation and the North Atlantic Oscillation. The time series of atmospheric moisture connections provided by Link](#)
436 [et al. \(2020\) allowed to study inter-annual variation in relatively local recycling. This shows that recycling is dependent on](#)
437 [multi-year atmospheric phenomena. During the major El Niño event of 2015-2016, the northeast of South Africa had a lower-](#)
438 [than-average local recycling ratio \(Fig. A11\) for 2015. This pattern coincides with the impact of wetness during El Niño years,](#)
439 [consistent with the hypothesis that wetness enhances LMR. Furthermore, strong events such as heat waves and droughts might](#)
440 [affect the multi-year annual mean. For example, we clearly find lower recycling over Russia during 2010, which may relate to](#)

441 [the 2010 heatwave in eastern Europe and Russia](#). Overall, for these multi-year and strong events we find that, for regions that
442 [face wetter-than-normal conditions, LMR is enhanced, and for regions that face drier-than-normal conditions, LMR is reduced](#).
443 [Hence, drought events might result in a decrease in LMR as seen for the 2010 heat wave event in Europe and Russia. However,](#)
444 [not for all inter-annual climate variability modes we find a clear impact on moisture recycling. It may be that these phenomena](#)
445 [do not affect wetness throughout the entire year, and therefore, annual means might not represent them well](#).

446 ~~4.5 Implications/applications of LMR Regardless of the importance of vertical shear in atmospheric moisture tracking~~
447 ~~models (Van der Ent et al., 2013) we do not find a clear correlation between local moisture recycling and vertical shear~~
448 ~~between 750 and 650 hPa. Shear is the friction between air layers that minimizes complete mixing, which for some~~
449 ~~regions around the world, is strongest between 650 and 750 hPa (Dominguez et al., 2016). A possible explanation is that~~
450 ~~due to its small spatial scale the temporal scale of LMR is also small, which causes the air not to reach 700 hPa within~~
451 ~~the spatial scale of LMR. Furthermore, it is possible that our study design is insufficient to capture the relation between~~
452 ~~LMR and shear throughout the year over the globe. We aim for a general analysis to identify the main drivers of LMR.~~
453 ~~A more detailed study that distinguishes seasons and different climate zones is necessary to identify more drivers. The~~
454 ~~spatial patterns of LMR, obtained in our study, resemble the spatial patterns of the regional recycling ratio (LMR is~~
455 ~~smaller than regional recycling) obtained by Van der Ent & Savenije (2011), who estimated average regional recycling~~
456 ~~ratios within a 1.5° grid cells globally between 1999 and 2008, using a Eulerian moisture tracking model. Due to~~
457 ~~different model set up and grid cell sizes, differences in the magnitude of recycling are expected; hence, here we only~~
458 ~~look at the qualitative patterns.~~

459 [LMR could be applied in the field of water management](#). The spatial pattern of LMR shows some overlap with global
460 agricultural water management (Molden, 2007; Salmon [et al., Friedl, Frohling, Wisser, & Douglas, 2015](#)) ([Salmon et al., 2015](#)).
461 Generally, the tropics have a high LMR and ~~mainly rainfed~~ agriculture [is mainly rainfed](#) (Salmon et al., 2015; Costa et al.,
462 2019), indicating [that](#) these agricultural regions are self-dependent [to some extent regarding concerning rainfall-precipitation](#)
463 ~~to some extent~~. Also, agriculture in the Mediterranean Basin and South Australia is mainly rainfed. For semi-arid regions [that](#)
464 dependent on rainfed agriculture, changes in precipitation may ~~might~~ have a significant impact (Keys et al., 2016). LMR in the
465 Mediterranean basin exceeds LMR in ~~s~~Southern Australia, indicating that a larger fraction of evaporated moisture returns
466 locally. Thus, when evaporation is maintained in the Mediterranean Basin, part of the precipitation will sustain here, which
467 holds to a lesser extent for ~~s~~Southern Australia. Besides LMR (i.e., local evaporation recycling), local precipitation recycling
468 can help to ~~fully~~ understand the precipitation dependence ~~ce~~ on local evaporation for each region. Irrigated agriculture is
469 important in India and China (Salmon et al., 2015; Döll and Siebert, 2002), which are regions with a relatively low LMR,
470 indicating that only a small amount of the evaporated moisture returns as [rainfall-precipitation](#) locally. For irrigated agriculture
471 in regions that are characterized by a high LMR, a relatively large amount of the evaporated water returns to its source, which
472 reduces the amount of water that is necessary for irrigation. Terrestrial evaporation is an important source for precipitation and
473 freshwater availability (Keune and Miralles, 2019). Therefore, spatial planning using LMR might improve agricultural water
474 management.

475
476
477

478 Global climate change likely affects atmospheric moisture connections due to changes in atmospheric dynamics. For example,
479 due to global warming, tropical atmospheric circulation may weaken (Vecchi et al., 2006), and the Hadley cells may move
480 poleward (Shaw, 2019), which will affect the updraft and downdraft of air around the globe, which we found to be ~~an~~ important
481 ~~driver of processes underlying~~ LMR. Furthermore, climate change has different opposing impacts on storm tracks which have
482 an important role in moisture transport by transporting latent heat poleward (Shaw et al., 2016). Furthermore, in a warmer
483 climate continental recycling is predicted to decrease and precipitation over land would be more dependent on evaporation
484 over the ocean (Findell et al., 2019). However, our study does not account for any impacts of climate change. As our results
485 indicate that wetness and convection enhance LMR, LMR ~~may will likely~~ change due to, for example, drying and wetting of
486 regions, changes in Hadley cell circulation, and circulation in the tropics.

487
488 Furthermore, climate change enhances the risk of droughts (Rasmijn et al., 2018; Teuling, 2018) and LMR might be used to
489 study drought resilience globally. ~~Drought can result in arid like conditions, which may lead to a decrease in LMR (Fig. 3).~~
490 ~~High LMR means that the local water cycle is relatively strong; therefore, a drought in a remote location is expected to have a~~
491 ~~small impact locally. However~~ As for a high LMR, a local drought might drastically impact the local water cycle.

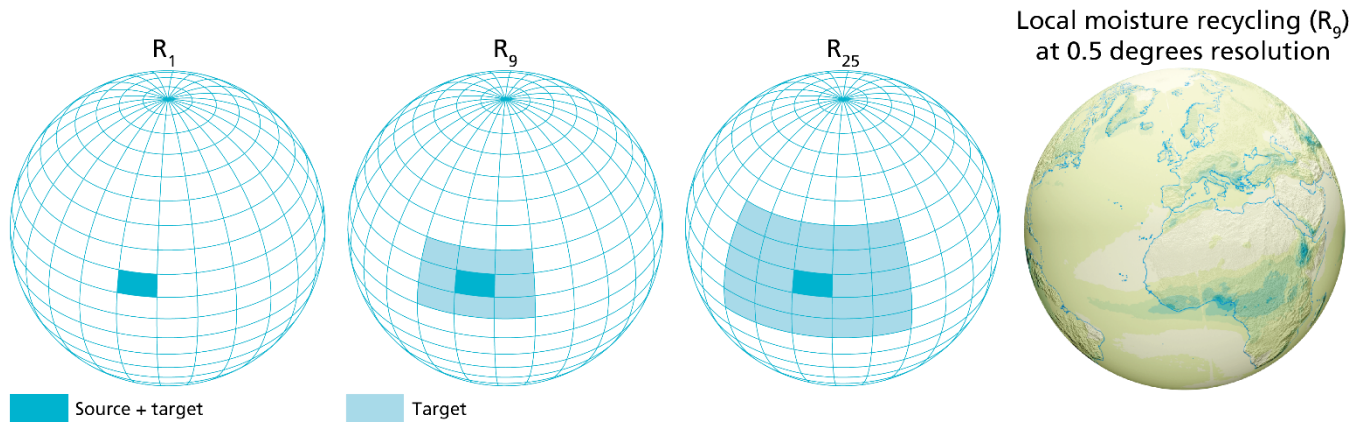
492
493 We expect that LMR can be helpful also in other ways. Specifically, we expect the concept of LMR can be used to study how
494 changes in evaporation, due to for example afforestation, affect the local water cycle beyond merely a loss of moisture ~~We~~
495 ~~expect that the novel concept of LMR can be helpful in various ways, but specifically it can be used to study how changes in~~
496 ~~evaporation because of for example afforestation, affect the local water cycle beyond merely a loss of moisture. However,~~
497 ~~besides evaporation, land-use changes also influence the energy balance and other factors that might alter the atmospheric~~
498 ~~moisture connections and thus, LMR. Using future land use scenarios as input for moisture tracking models, it will be possible~~
499 ~~to study the impact of land-use changes on atmospheric moisture connections. However, future scenarios often include other~~
500 ~~changes besides land use, which makes it possible to study the changes of land use specifically. However~~ Thus, LMR can help
501 us better predict the impact of land cover changes on the local water cycle. It might help us identify regions where reforestation
502 ~~would~~ does not cause local drying due to enhanced evaporation (Hoek van Dijke et al., 2022; Tuinenburg et al., ~~Bosmans, &~~
503 ~~Staal,~~ 2022). ~~(Dijke et al., 2022; Tuinenburg et al., 2022).~~ Overall, LMR gives us better insight into the atmospheric part of
504 the local water cycle and ~~can be used to contemplate~~ terrestrial evaporation as a source for local freshwater availability.

505 5 Conclusions

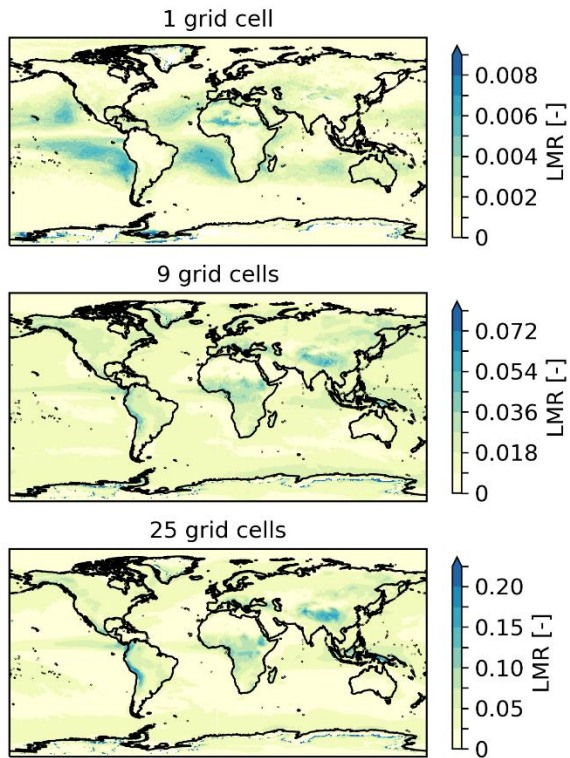
506 We calculated the local moisture recycling ratio (LMR) from atmospheric moisture connections at a spatial scale of 0.5°. LMR
507 is the fraction of evaporated moisture that ~~rains out~~ precipitates within a distance of 0.5° (typically 50 km) from its
508 source ~~approximately 50 km of its source location~~. On average, 1.76% (st.dev. = 1.1%) of global terrestrial evaporation returns
509 as rainfall precipitation locally, with peaks of approximately 6%. LMR peaks in summer and in wet and elevated regions. We

510 ~~identify~~ find that orography, precipitation, wetness, convective available potential energy, and wind affect LMR. In addition,
511 latitude correlates with LMR, which likely indicates the importance of the ascending air and descending air related to the
512 Hadley cell circulation. Furthermore, by comparing LMR calculated using different models we found that the spatial pattern
513 of LMR is not model-dependent, yet, the magnitude of LMR is strongly dependent on the model. ~~latitude, and convective~~
514 ~~available potential energy as main drivers of LMR~~. LMR ~~determines~~ defines the local impacts of enhanced evaporation on
515 precipitation and thus its role as a source for local freshwater availability. Therefore, LMR can be used to evaluate which
516 locations may be suitable for greening without largely disrupting the local water cycle. ~~Overall, LMR can be~~

517 Appendix A



518
519 **Figure A1.** Three definitions of the local moisture recycling ratio (LMR) from left to right: r_1 describes the fraction of evaporated
520 moisture that returns as precipitation in its source grid cell, r_9 describes the fraction of evaporated moisture that returns as
521 precipitation in its source grid cell and 8 neighbouring grid cells, and r_{25} describes the fraction of evaporated moisture that returns
522 as precipitation in its source grid cell and 24 neighbouring grid cells. LMR is calculated on a spatial scale of 0.5° and the first three
523 plots do not have a similar resolution. The plot on the right shows LMR on a spatial scale of 0.5° which is the resolution at which we
524 calculate all definitions (r_1 , r_9 and r_{25}).

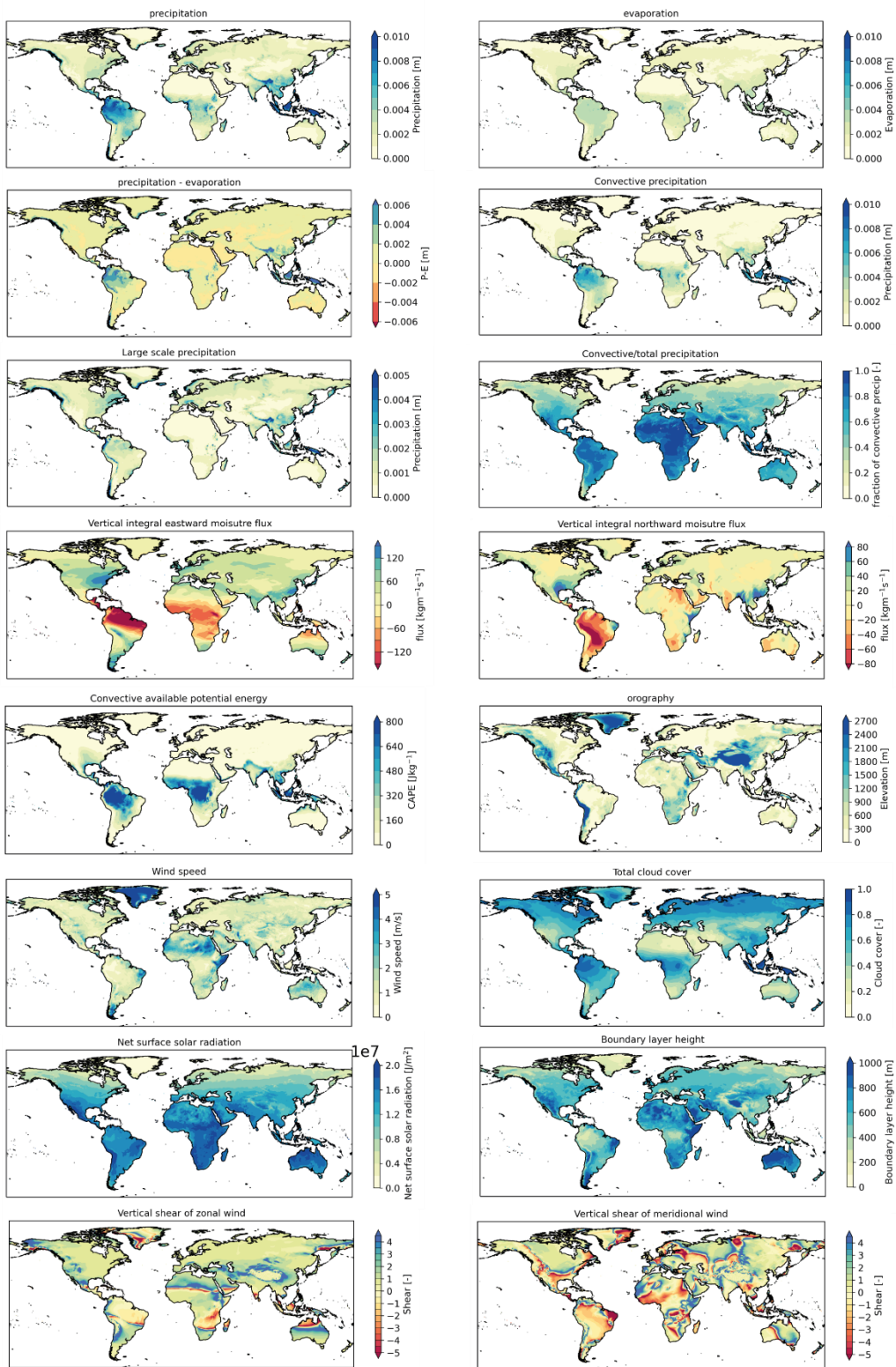


525

526 [Figure A2. 10-year climatology \(2008–2017\) of the three definitions of the local moisture recycling ratio \(LMR\). The top panel](#)
 527 [indicates the fraction of evaporated moisture that precipitates within its source grid cell \(\$r_1\$ \), the middle panel shows the fraction of](#)
 528 [evaporated moisture that precipitates within its source grid cell and its 8 neighbouring grid cells \(\$r_9\$ \), and the lower panel shows the](#)
 529 [fraction of evaporated moisture that precipitates within its source grid cell and its 24 neighbouring grid cells \(\$r_{25}\$ \).](#)

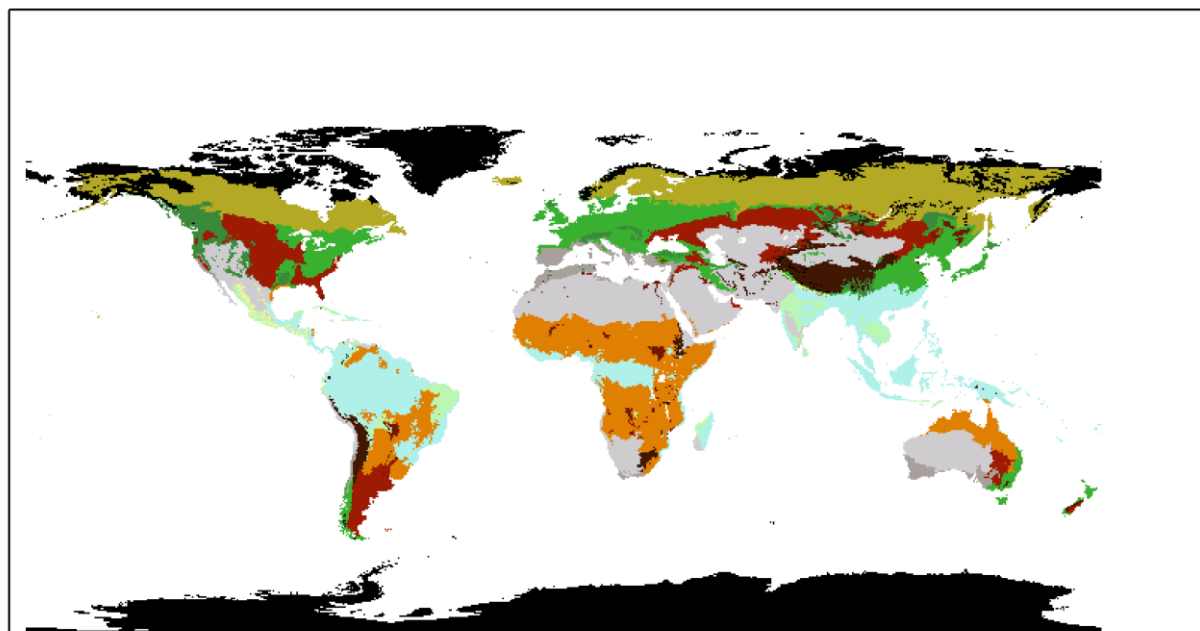
530 **Table A1: Defined classes for spearman rank correlation analysis.**

<i>Class</i>	Latitude ranges
1	-15°:15°
2	-30°:-15° and 15°:30°
3	-45°:-30° and 30°:45°
4	-60°:-45° and 45°:60°
5	60°:75°
6	75°:90°



532 [Figure A3. Global 10-year climatology \(2008–2017\) of \(from top to bottom and left to right\) precipitation, evaporation, precipitation](#)
 533 [– evaporation, convective precipitation, large-scale precipitation, fraction of convective precipitation, vertical integral of moisture](#)
 534 [flux in eastward direction, vertical integral of moisture flux in northward direction, CAPE, orography, vertical shear \(between 650](#)
 535 [and 750 hPa\) of zonal wind, and vertical shear \(between 650 and 750 hPa\) of meridional wind.](#)

536



Global Biomes

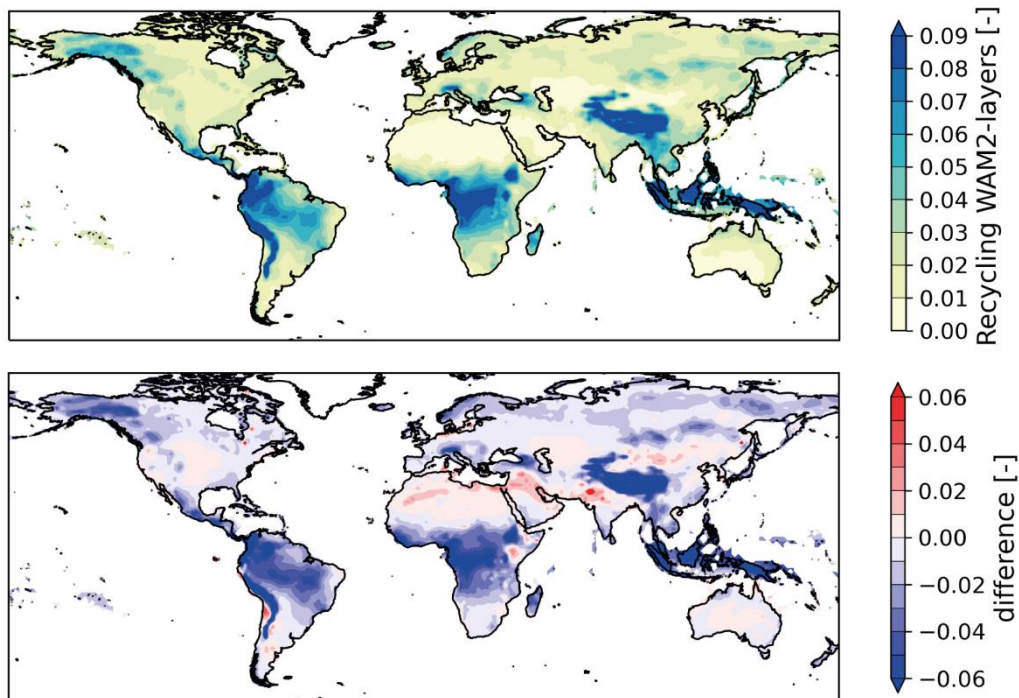
Value

- | | | | |
|---|--|---|---|
|  | Tropical and subtropical moist broadleaf forests |  | Tropical subtropical grasslands savannas and shrublands |
|  | Tropical and subtropical dry broadleaf forests |  | Temperate grasslands savannas and shrublands |
|  | Tropical and subtropical coniferous forests |  | Flooded grasslands and savannas |
|  | Temperate broadleaf and mixed forests |  | Montane grasslands and savannas |
|  | Temperate conifer forests |  | Tundra |
|  | Boreal forests/Taiga |  | Mediterranean forests woodlands and scrub |
| | |  | Deserts and Xeric shrublands |
| | |  | Mangroves |

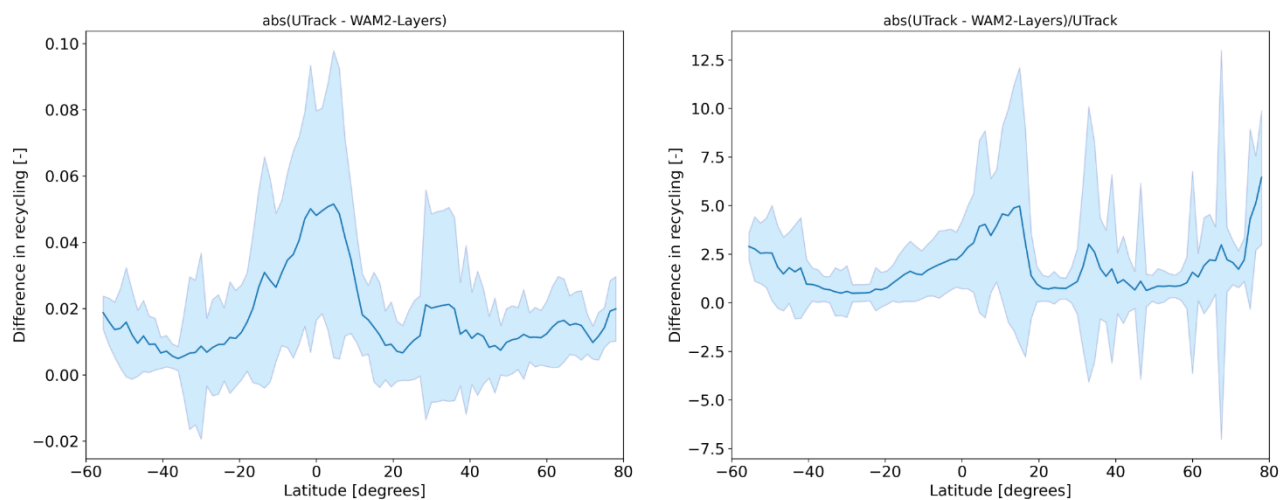
537

538 **Figure A24.** Major global biomes Ecoregions 2017 (<https://ecoregions.appspot.com/>).

539

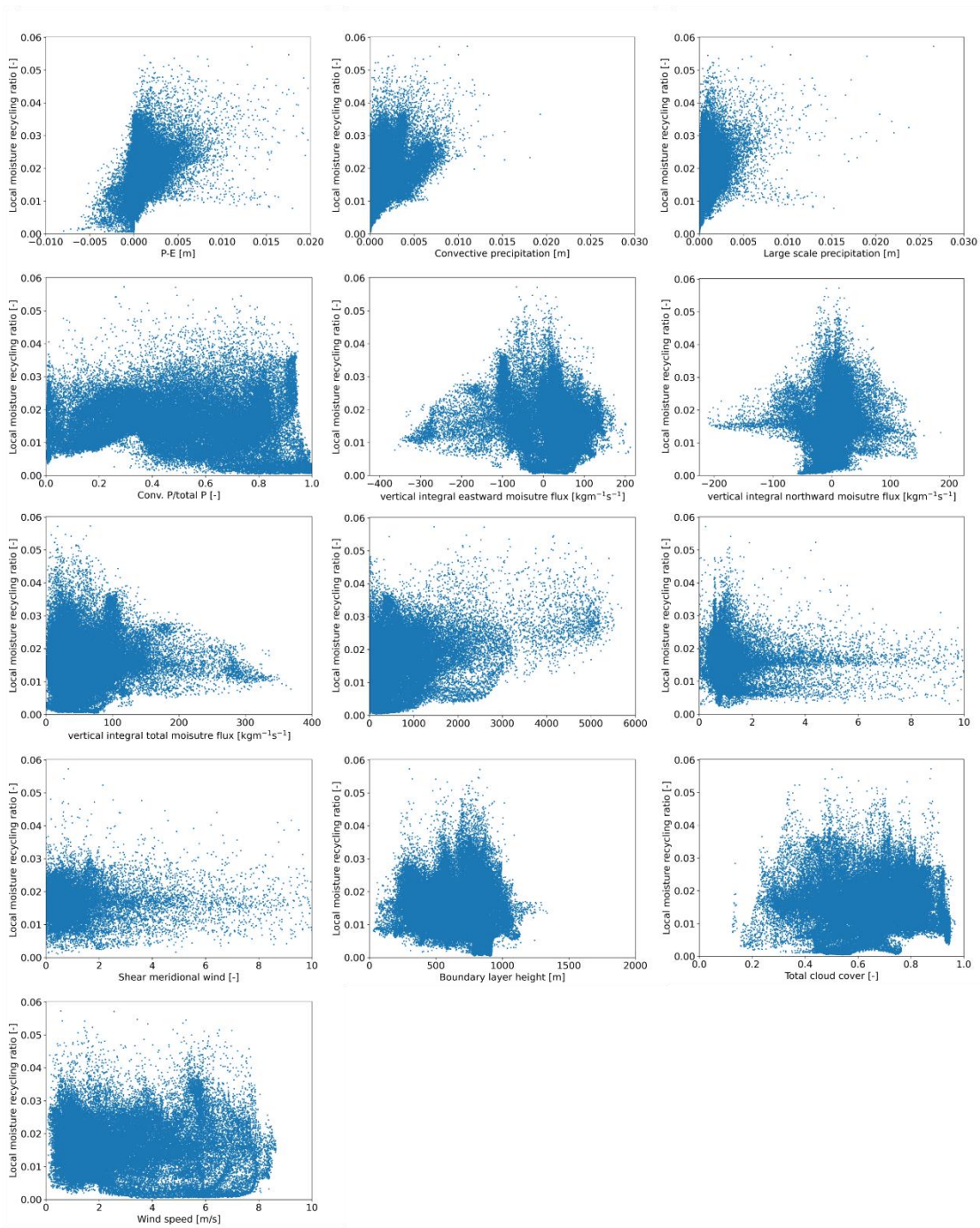


540
 541 **Figure A5. The 10-year climatology (2008-2017) of the recycling within one grid cell calculated with the dataset by (Link et al.,**
 542 **(2020), i.e., the output from the Eulerian moisture tracking model WAM2-layers (top) and the difference with the The 10-year**
 543 **climatology (2008-2017) of the recycling within one grid cell calculated with the dataset by (Tuinenburg et al., (2020).**
 544



545
 546 **Figure A6. The zonal mean of the absolute difference (left) and relative difference (right) between r_{UTrack} and $r_{WAM2-layers}$ (calculated**
 547 **as r_{UTrack} minus $r_{WAM2-layers}$, indicated by the blue line) and its standard deviation (blue area).**
 548

549 **Figure A4. Global multi-year (2008–2017) averaged maps of (from top to bottom and left to right) precipitation, evaporation,**
 550 **precipitation—evaporation, convective precipitation, large scale precipitation, fraction of convective precipitation, vertical integral**
 551 **of moisture flux in eastward direction, vertical integral of moisture flux in northward direction, CAPE, orography, vertical shear**
 552 **(between 650 and 750 hPa) of zonal wind, and vertical shear (between 650 and 750 hPa) of meridional wind.**



553

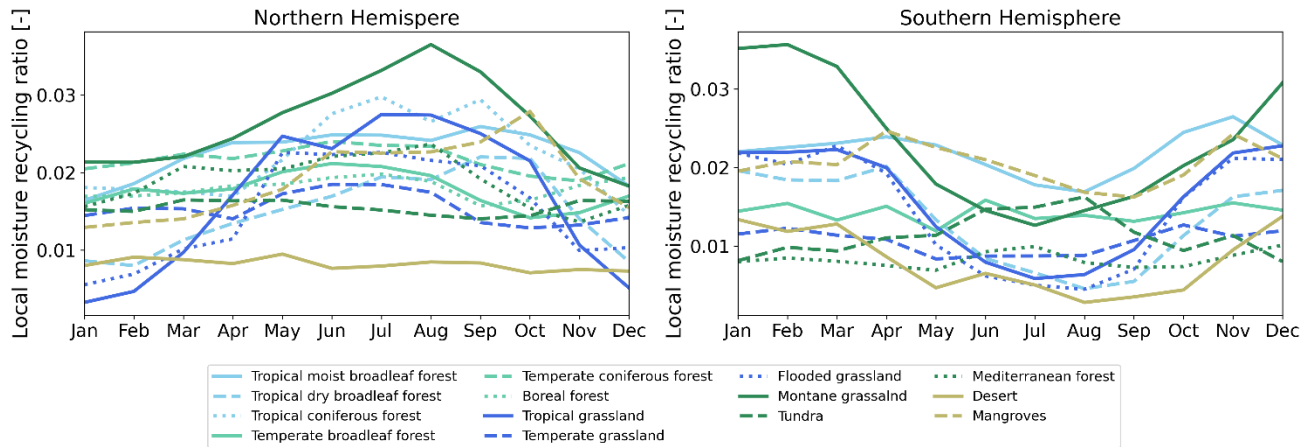
554

555 Figure A76. Scatter plots of the 10-year climatology -multi-year (2008–2017) of the averaged terrestrial local moisture recycling ratio
 556 and (from top to bottom and left to right) precipitation – evaporation, convective precipitation, large-scale precipitation, fraction of
 557 convective precipitation, vertical integral of moisture flux in eastward direction, vertical integral of moisture flux in northward
 558 direction, orography, vertical shear (between 650 and 750 hPa) of zonal wind, and vertical shear (between 650 and 750 hPa) of
 559 meridional wind, boundary layer height, total cloud cover, and wind speed. Each scatter represents one grid cell.

560 Table A2. Spearman rank correlation coefficients for additional variables at different latitude classes. ‘*’ indicates a significant
 561 correlation (p<0.05) and moderate and strong relations ($\rho>0.4$) are emboldened. The classes including latitudes between 0° and 60°
 562 include grid cells of the Northern Hemisphere and Southern Hemisphere. The classes including latitudes exceeding 60° include grid
 563 cells of the Northern Hemisphere only.

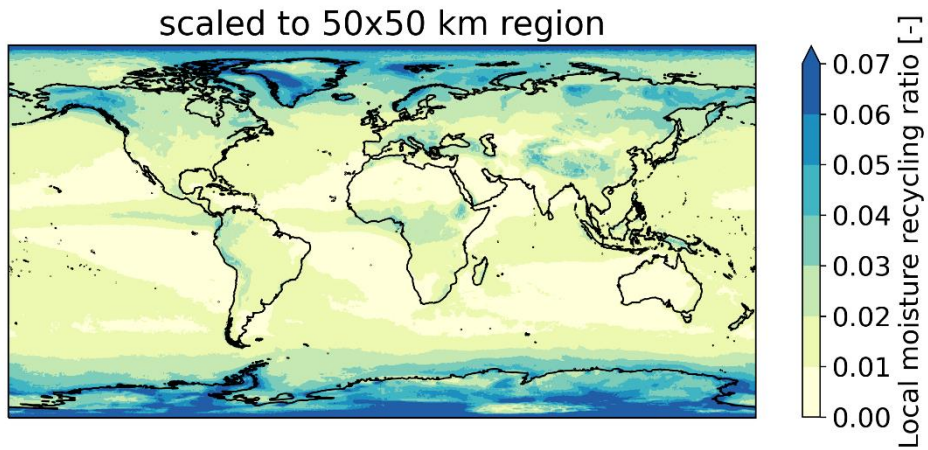
Variables	Spearman rank correlation coefficient					
	0°-15°	15°-30°	30°-45°	45°-60°	60°-75°	75°-90°
Total cloud cover and wind speed	-0.58	-0.41	-0.23	0.08	0.16	-0.51
Large-scale precipitation and wind speed	-0.30	-0.46	-0.37	0.06	0.11	-0.28
Convective precipitation and wind speed	-0.63	-0.50	-0.33	-0.13	-0.41	-0.61
Total cloud cover and precipitation	0.85	0.92	0.76	0.58	-0.08	0.46
Total cloud cover and convective precipitation	0.85	0.90	0.63	0.23	-0.09	0.67
Total cloud cover and large-scale precipitation	0.71	0.90	0.81	0.70	-0.02	0.43
LMR and wind speed at 650 hpa	0.26	-0.18	-0.37	-0.16	-0.15	-0.27
LMR and wind speed at 750 hpa	-0.09	0.023	-0.39	-0.19	-0.09	-0.31

564



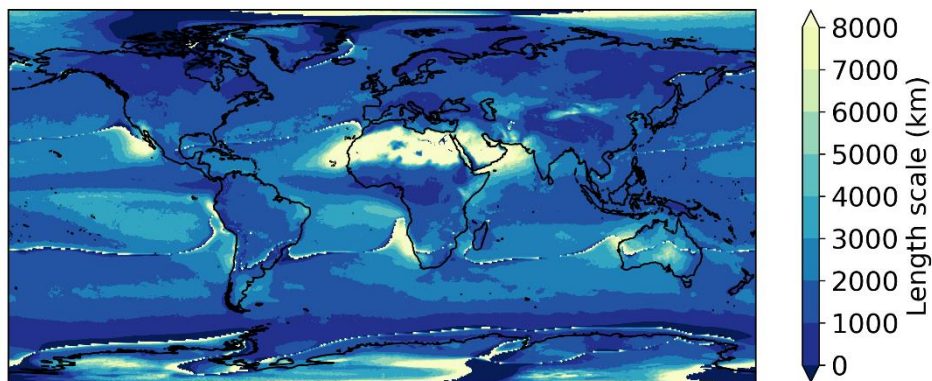
565

566 Figure A78. Time series of the local moisture recycling ratio for global biomes on the Northern (left) and Southern (right)
 567 Hemispheres. The plots show the 10-year climatology The values are multi-year (2008–2017) averages.



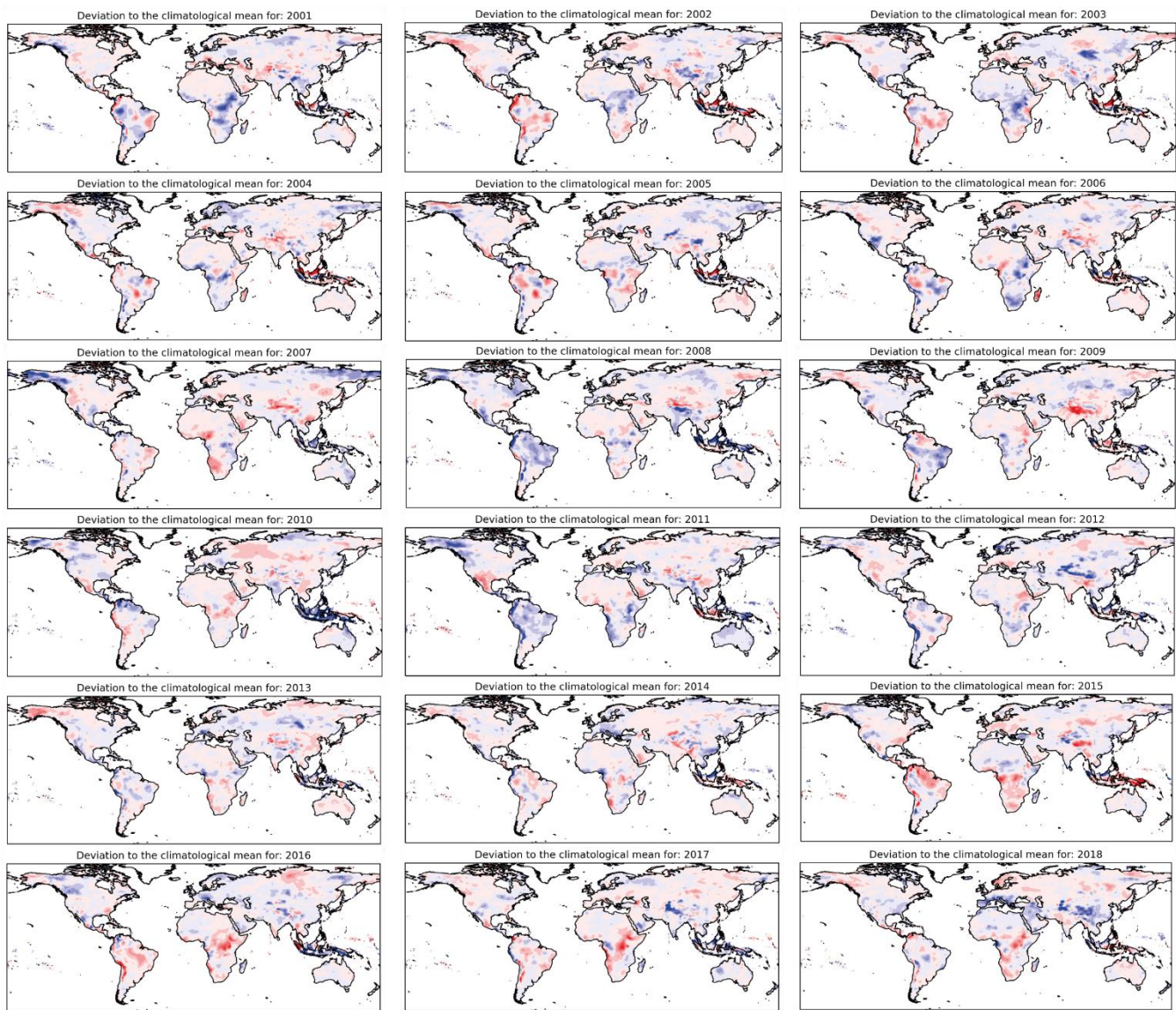
568

569 [Figure A9: The local moisture recycling ratio scaled to a grid cell size of 50 km x 50 km. The plot shows the 10-year climatology](#)
 570 [\(2008-2017\). We divided the original local moisture recycling ratio by the area of the grid cell and multiplied it with 2500 km²](#)



571

572 [Figure A10: Evaporation recycling length scale as defined by Van der Ent and Savenije \(2011\) for each grid cell of 0.5°x0.5°. The](#)
 573 [plot shows the average of 2008-2017.](#)



574

575 [Figure A11. Inter-annual variation of recycling within a single grid cell of 1.5° between 2001-2018. Each plot shows the](#)
 576 [difference between annual averaged recycling and the climatological mean of recycling. Data obtained from \(Link et](#)
 577 [al., \(2020\).](#)

578 **Code availability**

579 The code that was used to calculate the local moisture recycling ratio and for the analyses is available from the corresponding
580 author upon reasonable request.

581 **Data availability**

582 The atmospheric moisture connections from Tuinenburg et al., (2020) are available from the PANGAEA archive at 0.5 and
583 1.0 degrees resolution (<https://doi.pangaea.de/10.1594/PANGAEA.912710>).

584 The atmospheric moisture connections from Link et al., (2020) are available from the PANGAEA archive at 1.5 degrees
585 resolution (<https://doi.pangaea.de/10.1594/PANGAEA.908705>).

586 **Author contributions**

587 JT designed the study with contributions from all authors. JT carried out the research. JT wrote the first draft of the manuscript
588 in close collaboration with AS. All authors contributed to the discussion and the final version of the manuscript.

589 **Acknowledgements**

590 This work was performed in the cooperation framework of Wetsus, European Centre of Excellence for Sustainable Water
591 Technology (www.wetusus.eu). Wetusus is co-funded by the Dutch Ministry of Economic Affairs and Climate Policy, the
592 Northern Netherlands Provinces the Province of Fryslân. The authors would like to thank the participants of the natural water
593 production theme for the fruitful discussions and financial support. AS acknowledges support from the Talent Programme
594 grant VI.Veni.202.170 by the Dutch Research Council (NWO). OT acknowledges support from the research programme
595 Innovative Research Incentives Scheme Veni (016.veni.171.019), funded by the Dutch Research Council.

596 **References**

597 An, W., Hou, S., Zhang, Q., Zhang, W., Wu, S., Xu, H., Pang, H., Wang, Y., and Liu, Y.: Enhanced recent local moisture
598 recycling on the northwestern Tibetan Plateau deduced from ice core deuterium excess records, *J. Geophys. Res.-Atmos.*, 122,
599 12541–12556, <https://doi.org/10.1002/2017JD027235>, 2017.

600 Bagley, J. E., Desai, A. R., Dirmeyer, P. A., and Foley, J. A.: Effects of land cover change on moisture availability and potential
601 crop yield in the worlds breadbaskets, *Environ. Res. Lett.*, 7, 014009, <https://doi.org/10.1088/1748-9326/7/1/014009>, 2012.

602 Bagley, J. E., Desai, A. R., Harding, K. J., Snyder, P. K., and Foley, J. A.: Drought and deforestation: Has land cover change
603 influenced recent precipitation extremes in the Amazon?, *J. Clim.*, 27, 345–361, <https://doi.org/10.1175/JCLI-D-12-00369.1>,

604 2014.

605 Brown, A. E., Zhang, L., McMahon, T. A., Western, A. W., and Vertessy, R. A.: A review of paired catchment studies for
606 determining changes in water yield resulting from alterations in vegetation, *J. Hydrol.*, 310, 28–61,
607 <https://doi.org/10.1016/j.jhydrol.2004.12.010>, 2005.

608 Budyko, M. I.: *Climate and life*, Academic Press: New York, 1974.

609 Burde, G. I.: Bulk recycling models with incomplete vertical mixing. Part II: Precipitation recycling in the Amazon Basin, *J.*
610 *Clim.*, 19, 1461–1472, <https://doi.org/10.1175/JCLI3687.1>, 2006.

611 Burde, G. I. and Zangvil, A.: The estimation of regional precipitation recycling. Part I: Review of recycling models, *J. Clim.*,
612 14, 2509–2527, <https://doi.org/10.1175/1520-0442>, 2001.

613 Costa, M. H., Fleck, L. C., Cohn, A. S., Abrahão, G. M., Brando, P. M., Coe, M. T., Fu, R., Lawrence, D., Pires, G. F., Pousa,
614 R., and Soares-Filho, B. S.: Climate risks to Amazon agriculture suggest a rationale to conserve local ecosystems, *Front. Ecol.*
615 *Environ.*, 17, 584–590, <https://doi.org/10.1002/fee.2124>, 2019.

616 Cui, J., Lian, X., Huntingford, C., Gimeno, L., Wang, T., Ding, J., He, M., Xu, H., Chen, A., Gentine, P., and Piao, S.: Global
617 water availability boosted by vegetation-driven changes in atmospheric moisture transport, *Nat. Geosci.*, 15, 982–988,
618 <https://doi.org/10.1038/s41561-022-01061-7>, 2022.

619 Döll, P. and Siebert, S.: Global modeling of irrigation water requirements, *Water Resour. Res.*, 38, 1037,
620 <https://doi.org/10.1029/2001wr000355>, 2002.

621 Dominguez, F., Kumar, P., Liang, X. Z., and Ting, M.: Impact of atmospheric moisture storage on precipitation recycling, *J.*
622 *Clim.*, 19, 1513–1530, <https://doi.org/10.1175/JCLI3691.1>, 2006.

623 Dominguez, F., Miguez-Macho, G., and Hu, H.: WRF with water vapor tracers: A study of moisture sources for the North
624 American Monsoon, *J. Hydrometeorol.*, 17, 1915–1927, <https://doi.org/10.1175/JHM-D-15-0221.1>, 2016.

625 Dominguez, F., Hu, H., and Martinez, J. A.: Two-Layer Dynamic Recycling Model (2L-DRM): Learning from moisture
626 tracking models of different complexity, *J. Hydrometeorol.*, 21, 3–16, <https://doi.org/10.1175/jhm-d-19-0101.1>, 2020.

627 Eltahir, E. A. B.: A soil moisture-rainfall feedback mechanism, *Water Resour. Res.*, 34, 765–776, 1998.

628 Eltahir, E. A. B. and Pal, J. S.: Relationship between surface conditions and subsequent rainfall in convective storms, *J.*
629 *Geophys. Res.-Atmos.*, 101, 26237–26245, <https://doi.org/10.1029/96jd01380>, 1996.

630 Van der Ent, R. J. and Savenije, H. H. G.: Length and time scales of atmospheric moisture recycling, *Atmos. Chem. Phys.*, 11,
631 1853–1863, <https://doi.org/10.5194/acp-11-1853-2011>, 2011.

632 Van der Ent, R. J. and Savenije, H. H. G.: Oceanic sources of continental precipitation and the correlation with sea surface
633 temperature, *Water Resour. Res.*, 49, 3993–4004, <https://doi.org/10.1002/wrcr.20296>, 2013.

634 Van der Ent, R. J., Savenije, H. H. G., Schaeffli, B., and Steele-Dunne, S. C.: Origin and fate of atmospheric moisture over
635 continents, *Water Resour. Res.*, 46, W09525, <https://doi.org/10.1029/2010WR009127>, 2010.

636 Van der Ent, R. J., Tuinenburg, O. A., Knoche, H. R., Kunstmann, H., and Savenije, H. H. G.: Should we use a simple or
637 complex model for moisture recycling and atmospheric moisture tracking?, *Hydrol. Earth Syst. Sc.*, 17, 4869–4884,

638 <https://doi.org/10.5194/hess-17-4869-2013>, 2013.

639 Van der Ent, R. J., Wang-Erlandsson, L., Keys, P. W., and Savenije, H. H. G.: Contrasting roles of interception and
640 transpiration in the hydrological cycle - Part 2: Moisture recycling, *Earth Syst. Dynam.*, 5, 471–489,
641 <https://doi.org/10.5194/esd-5-471-2014>, 2014.

642 Falkenmark, M., Wang-Erlandsson, L., and Rockström, J.: Understanding of water resilience in the Anthropocene, *J. Hydrol.*,
643 2, 100009, <https://doi.org/10.1016/j.hydroa.2018.100009>, 2019.

644 Findell, K. L., Keys, P. W., van der Ent, R. J., Lintner, B. R., Berg, A., and Krasting, J. P.: Rising temperatures increase
645 importance of oceanic evaporation as a source for continental precipitation, *J. Clim.*, 32, 7713–7726,
646 <https://doi.org/10.1175/jcli-d-19-0145.1>, 2019.

647 Hersbach, H., Bell, B., Berrisford, P., Hirahara, S., Horányi, A., Muñoz-Sabater, J., Nicolas, J., Peubey, C., Radu, R., Schepers,
648 D., Simmons, A., Soci, C., Abdalla, S., Abellan, X., Balsamo, G., Bechtold, P., Biavati, G., Bidlot, J., Bonavita, M., De Chiara,
649 G., Dahlgren, P., Dee, D., Diamantakis, M., Dragani, R., Flemming, J., Forbes, R., Fuentes, M., Geer, A., Haimberger, L.,
650 Healy, S., Hogan, R. J., Hólm, E., Janisková, M., Keeley, S., Laloyaux, P., Lopez, P., Lupu, C., Radnoti, G., de Rosnay, P.,
651 Rozum, I., Vamborg, F., Villaume, S., and Thépaut, J. N.: The ERA5 global reanalysis, *Q. J. Roy. Meteor. Soc.*, 146, 1999–
652 2049, <https://doi.org/10.1002/qj.3803>, 2020.

653 Hoek van Dijke, A. J., Herold, M., Mallick, K., Benedict, I., Machwitz, M., Schlerf, M., Pranindita, A., Theeuwens, J. J. E.,
654 Bastin, J.-F., and Teuling, A. J.: Shifts in regional water availability due to global tree restoration, *Nat. Geosci.*, 15, 363–368,
655 <https://doi.org/10.1038/s41561-022-00935-0>, 2022.

656 Jackson, R. B., Jobbágy, E. G., Avissar, R., Roy, S. B., Barrett, D. J., Cook, C. W., Farley, K. A., Le Maitre, D. C., McCarl,
657 B. A., and Murray, B. C.: Atmospheric science: Trading water for carbon with biological carbon sequestration, *Science* (80-
658), 310, 1944–1947, <https://doi.org/10.1126/science.1119282>, 2005.

659 Jana, S., Rajagopalan, B., Alexander, M. A., and Ray, A. J.: Understanding the dominant sources and tracks of moisture for
660 summer rainfall in the southwest united states, *J. Geophys. Res.-Atmos.*, 123, 4850–4870,
661 <https://doi.org/10.1029/2017JD027652>, 2018.

662 Keune, J. and Miralles, D. G.: A precipitation recycling network to assess freshwater vulnerability: Challenging the watershed
663 convention, *Water Resour. Res.*, 55, 9947–9961, <https://doi.org/10.1029/2019WR025310>, 2019.

664 Keune, J., Schumacher, D. L., and Miralles, D. G.: A unified framework to estimate the origins of atmospheric moisture and
665 heat using Lagrangian models, *Geosci. Model Dev.*, 15, 1875–1898, <https://doi.org/10.5194/gmd-15-1875-2022>, 2022.

666 Keys, P. W., Van der Ent, R. J., Gordon, L. J., Hoff, H., Nikoli, R., and Savenije, H. H. G.: Analyzing precipitationsheds to
667 understand the vulnerability of rainfall dependent regions, *Biogeosciences*, 9, 733–746, [https://doi.org/10.5194/bg-9-733-](https://doi.org/10.5194/bg-9-733-2012)
668 2012, 2012.

669 Keys, P. W., Barnes, E. A., van der Ent, R. J., and Gordon, L. J.: Variability of moisture recycling using a precipitationshed
670 framework, *Hydrol. Earth Syst. Sc.*, 18, 3937–3950, <https://doi.org/10.5194/hess-18-3937-2014>, 2014.

671 Keys, P. W., Wang-Erlandsson, L., and Gordon, L. J.: Revealing invisible Water: Moisture recycling as an ecosystem service,

672 PLoS One, 11, e0151993, <https://doi.org/10.1371/journal.pone.0151993>, 2016.

673 Keys, P. W., Porkka, M., Wang-Erlandsson, L., Fetzer, I., Gleeson, T., and Gordon, L. J.: Invisible water security: Moisture
674 recycling and water resilience, *Water Secur.*, 8, 57–89, <https://doi.org/10.1016/j.wasec.2019.100046>, 2019.

675 Knox, R., Bisht, G., Wang, J., and Bras, R.: Precipitation variability over the forest-to-nonforest transition in Southwestern
676 Amazonia, *J. Clim.*, 24, 2368–2377, <https://doi.org/10.1175/2010JCLI3815.1>, 2011.

677 Lettau, H., K., L., and Molion, L. C. B.: Amazonia’s hydrologic cycle and the role of atmospheric recycling in assessing
678 deforestation effects., *Mon. Weather Rev.*, 107, 227–238, 1979.

679 Liberato, M. L. R., Ramos, A. M., Trigo, R. M., Trigo, I. F., Durán-Quesada, A. M., Nieto, R., and Gimeno, L.: Moisture
680 sources and large-scale dynamics associated with a flash flood event, *Geoph. Monog. Ser.*, 200, 111–126,
681 <https://doi.org/10.1029/2012GM001244>, 2012.

682 Link, A., Van Der Ent, R., Berger, M., Eisner, S., and Finkbeiner, M.: The fate of land evaporation - A global dataset, *Earth
683 Syst. Sci. Data*, 12, 1897–1912, <https://doi.org/10.5194/essd-12-1897-2020>, 2020.

684 Molden, D.: *A Comprehensive Assessment of Water Management in Agriculture; Summary*, 40 pp., 2007.

685 O’Connor, J. C., Dekker, S. C., Staal, A., Tuinenburg, O. A., Rebel, K. T., and Santos, M. J.: Forests buffer against variations
686 in precipitation, *Glob. Chang. Biol.*, 27, 4686–4696, <https://doi.org/10.1111/gcb.15763>, 2021.

687 Pranindita, A., Wang-Erlandsson, L., Fetzer, I., and Teuling, A. J.: Moisture recycling and the potential role of forests as
688 moisture source during European heatwaves, *Clim. Dynam.*, 58, 609–624, <https://doi.org/10.1007/s00382-021-05921-7>, 2022.

689 Rasmijn, L. M., Van Der Schrier, G., Bintanja, R., Barkmeijer, J., Sterl, A., and Hazeleger, W.: Future equivalent of 2010
690 Russian heatwave intensified by weakening soil moisture constraints, *Nat. Clim. Chang.*, 8, 381–385,
691 <https://doi.org/10.1038/s41558-018-0114-0>, 2018.

692 Richards, F. and Arkin, P.: On the Relationship between Satellite-Observed Cloud Cover and Precipitation, *Mon. Weather
693 Rev.*, 109, 1081–1093, 1998.

694 Roe, G. H.: Orographic precipitation, *Annu. Rev. Earth. Pl. Sc.*, 33, 645–671,
695 <https://doi.org/10.1146/annurev.earth.33.092203.122541>, 2005.

696 Salmon, J. M., Friedl, M. A., Frohling, S., Wisser, D., and Douglas, E. M.: Global rain-fed, irrigated, and paddy croplands: A
697 new high resolution map derived from remote sensing, crop inventories and climate data, *Int. J Appl. Earth. Obs.*, 38, 321–
698 334, <https://doi.org/10.1016/j.jag.2015.01.014>, 2015.

699 Scheff, J. and Frierson, D.: Twenty-First-Century multimodel subtropical precipitation declines are mostly midlatitude shifts,
700 *J. Clim.*, 25, 4330–4347, <https://doi.org/10.1175/JCLI-D-11-00393.1>, 2012.

701 Shaw, T. A.: Mechanisms of future predicted changes in the zonal mean mid-latitude circulation, *Curr. Clim. Chang. Reports*,
702 5, 345–357, <https://doi.org/10.1007/s40641-019-00145-8>, 2019.

703 Shaw, T. A., Baldwin, M., Barnes, E. A., Caballero, R., Garfinkel, C. I., Hwang, Y. T., Li, C., O’Gorman, P. A., Rivière, G.,
704 Simpson, I. R., and Voigt, A.: Storm track processes and the opposing influences of climate change, *Nat. Geosci.*, 9, 656–664,
705 <https://doi.org/10.1038/ngeo2783>, 2016.

706 Sodemann, H.: Beyond turnover time: Constraining the lifetime distribution of water vapor from simple and complex
707 approaches, *J. Atmos. Sci.*, 77, 413–433, <https://doi.org/10.1175/JAS-D-18-0336.1>, 2020.

708 Staal, A., Tuinenburg, O. A., Bosmans, J. H. C., Holmgren, M., Van Nes, E. H., Scheffer, M., Zemp, D. C., and Dekker, S. C.:
709 Forest-rainfall cascades buffer against drought across the Amazon, *Nat. Clim. Chang.*, 8, 539–543,
710 <https://doi.org/10.1038/s41558-018-0177-y>, 2018.

711 Staal, A., Flores, B. M., Aguiar, A. P. D., Bosmans, J. H. C., Fetzer, I., and Tuinenburg, O. A.: Feedback between drought and
712 deforestation in the Amazon, *Environ. Res. Lett.*, 15, 044024, <https://doi.org/10.1088/1748-9326/ab738e>, 2020.

713 Stohl, A., Forster, C., Frank, A., Seibert, P., and Wotawa, G.: Technical note: The Lagrangian particle dispersion model
714 FLEXPART version 6.2, *Atmos. Chem. Phys.*, 5, 2461–2474, <https://doi.org/10.5194/acp-5-2461-2005>, 2005.

715 Taylor, C. M., de Jeu, R. A. M., Guichard, F., Harris, P. P., and Dorigo, W. A.: Afternoon rain more likely over drier soils,
716 *Nature*, 489, 423–426, <https://doi.org/10.1038/nature11377>, 2012.

717 Teuling, A. J.: A hot future for European droughts, *Nat. Clim. Chang.*, 8, 364–365, <https://doi.org/10.1038/s41558-018-0154->
718 5, 2018.

719 Trenberth, K. E.: Atmospheric moisture recycling: Role of advection and local evaporation, *J. Clim.*, 12, 1368–1381,
720 [https://doi.org/10.1175/1520-0442\(1999\)012<1368:amroa>2.0.co;2](https://doi.org/10.1175/1520-0442(1999)012<1368:amroa>2.0.co;2), 1999.

721 Tuinenburg, O. A. and Staal, A.: Tracking the global flows of atmospheric moisture and associated uncertainties, *Hydrol. Earth*
722 *Syst. Sc.*, 24, 2419–2435, <https://doi.org/10.5194/hess-24-2419-2020>, 2020.

723 Tuinenburg, O. A., Hutjes, R. W. A., and Kabat, P.: The fate of evaporated water from the Ganges basin, *J. Geophys. Res.-*
724 *Atmos.*, 117, 1–17, <https://doi.org/10.1029/2011JD016221>, 2012.

725 Tuinenburg, O. A., Theeuwens, J. J. E., and Staal, A.: High-resolution global atmospheric moisture connections from
726 evaporation to precipitation, *Earth Syst. Sci. Data*, 12, 3177–3188, <https://doi.org/10.5194/essd-12-3177-2020>, 2020.

727 Tuinenburg, O. A., Bosmans, J. H. C., and Staal, A.: The global potential of forest restoration for drought mitigation, *Environ.*
728 *Res. Lett.*, 17, 034045, <https://doi.org/10.1088/1748-9326/ac55b8>, 2022.

729 Vecchi, G. A., Soden, B. J., Wittenberg, A. T., Held, I. M., Leetmaa, A., and Harrison, M. J.: Weakening of tropical Pacific
730 atmospheric circulation due to anthropogenic forcing, *Nature*, 441, 73–76, <https://doi.org/10.1038/nature04744>, 2006.

731 Wallace, J. M. and Hobbs, P. V.: *Atmospheric science: an introductory survey*, 2nd ed., Elsevier, 2006.

732 Wang-Erlandsson, L., Fetzer, I., Keys, P. W., van der Ent, R. J., Savenije, H. H. G., and Gordon, L. J.: Remote land use impacts
733 on river flows through atmospheric teleconnections, *Hydrol. Earth Syst. Sc.*, 22, 4311–4328, <https://doi.org/10.5194/hess-22->
734 4311-2018, 2018.

735 Wang-Erlandsson, L., Tobian, A., van der Ent, R. J., Fetzer, I., te Wierik, S., Porkka, M., Staal, A., Jaramillo, F., Dahlmann,
736 H., Singh, C., Greve, P., Gerten, D., Keys, P. W., Gleeson, T., Cornell, S. E., Steffen, W., Bai, X., and Rockström, J.: A
737 planetary boundary for green water, *Nat. Rev. Earth Environ.*, 3, 380–392, <https://doi.org/10.1038/s43017-022-00287-8>, 2022.

738 Wang, C. and Yang, K.: Changes in the moisture contribution over global arid regions, *Clim. Dynam.*, 1–15,
739 <https://doi.org/10.1007/s00382-022-06600-x>, 2022.

740 te Wierik, S. A., Cammeraat, E. L. H., Gupta, J., and Artzy-Randrup, Y. A.: Reviewing the impact of land use and land-use
741 change on moisture recycling and precipitation patterns, *Water Resour. Res.*, 57, e2020WR029234,
742 <https://doi.org/10.1029/2020WR029234>, 2021.

743 Te Wierik, S. A., Gupta, J., Cammeraat, E. L. H., and Artzy-Randrup, Y. A.: The need for green and atmospheric water
744 governance, *Wiley Interdiscip. Rev. Water*, 7, e1406, <https://doi.org/10.1002/wat2.1406>, 2020.

745 Williams, E. and Renno, N.: An analysis of the conditional instability of the tropical atmosphere, *Mon. Weather Rev.*, 121,
746 21–35, 1993.

747 Wunderling, N., Wolf, F., Tuinenburg, O. A., and Staal, A.: Network motifs shape distinct functioning of Earth’s moisture
748 recycling hubs, *Nat. Commun.*, 13, 6574, <https://doi.org/10.1038/s41467-022-34229-1>, 2022.

749